Journal of Vertebrate Paleontology

ISSN: (Print) (Online) Journal homepage: https://www.tandfonline.com/loi/ujvp20

Computed tomography and three-dimensional reconstruction of the skull of the stem tetrapod *Crassigyrinus scoticus* Watson, 1929

Laura B. Porro, Emily J. Rayfield & Jennifer A. Clack

To cite this article: Laura B. Porro, Emily J. Rayfield & Jennifer A. Clack (2022) Computed tomography and three-dimensional reconstruction of the skull of the stem tetrapod *Crassigyrinus scoticus* Watson, 1929, Journal of Vertebrate Paleontology, 42:4, e2183134, DOI: 10.1080/02724634.2023.2183134

To link to this article: https://doi.org/10.1080/02724634.2023.2183134

Journal of Vertebrate Paleontology e2183134 (31 pages)
Published with license by the Society of Vertebrate Paleontology
DOI: 10.1080/02724634.2023.2183134

ARTICLE

COMPUTED TOMOGRAPHY AND THREE-DIMENSIONAL RECONSTRUCTION OF THE SKULL OF THE STEM TETRAPOD *CRASSIGYRINUS SCOTICUS* WATSON, 1929

LAURA B. PORRO, [1,2*] EMILY J. RAYFIELD, [2] and JENNIFER A. CLACK [3†]
[1]Centre for Integrative Anatomy, Department of Cell and Developmental Biology, UCL, Anatomy Building, Gower Street, London WC1E 6BT, U.K., l.porro@ucl.ac.uk;
[2]School of Earth Sciences, University of Bristol, Life Sciences Building, 24 Tyndall Avenue, Bristol BS8 1TQ, U.K., e.rayfield@bristol.ac.uk;
[3]University Museum of Zoology, University of Cambridge, Downing Street, Cambridge CB2 3EJ, U.K.

ABSTRACT—The early tetrapod *Crassigyrinus scoticus* was a large aquatic predator known from the lower- to mid-Carboniferous (upper Tournasian to upper Visean/lower Serpukovian, approximately 350–330 Ma) of Scotland and Canada. *Crassigyrinus* is enigmatic in terms of its phylogenetic position due to its unusual morphology, which features a mixture of primitive and derived characters. Previous reconstructions, based on five incomplete and deformed specimens, have suggested a dorsoventrally tall skull with a short and broad snout, large orbits and external nares, and an extended postorbital region. In this study, we scanned four specimens using computed tomography and segmented imaging data to separate bone from matrix and individual bones from each other. Based on these data, we present a revised description of the upper and lower jaws, including sutural morphology and abundant new anatomical information. Damage was repaired and the skull retrodeformed to create a hypothetical three-dimensional reconstruction of the skull of *Crassigyrinus* that is dorsoventrally flatter than earlier reconstructions, yet still morphologically unique amongst early tetrapods. Overall skull shape, the size and distribution of the teeth, sutural morphology, and the specialized anatomy of the jaw joint and mandibular symphysis all suggest that *Crassigyrinus* was a powerful aquatic predator capable of hunting and subduing large prey.

SUPPLEMENTAL DATA—Supplemental materials are available for this article for free at www.tandfonline.com/UJVP.

Citation for this article: Porro, L. B., E. J. Rayfield, and J. A. Clack. (2023) Computed tomography and three-dimensional reconstruction of the skull of the stem tetrapod *Crassigyrinus scoticus* Watson, 1929. *Journal of Vertebrate Paleontology*. https://doi.org/10.1080/02724634.2023.2183134

Submitted: July 1, 2022
Revisions received: January 20, 2023
Accepted: January 20, 2023
First published online: May 2, 2023

INTRODUCTION

The invasion of the land by vertebrates in the Late Devonian and Carboniferous was a landmark event in the history of life, classically depicted as the gradual acquisition of terrestrial adaptations by early tetrapods (Clack, 1998b, 2003; Coates, 1996; Gregory & Raven, 1941; Jarvik, 1980). Over the past 30 years, new fossil discoveries (Ahlberg, 1995; Ahlberg et al., 1994; Beznosov et al., 2019; Clack, 2002a; Coates & Clack, 1990; Daeschler et al., 2006), revised anatomical interpretations (Ahlberg et al., 2005; Boisvert et al., 2008; Coates, 1996), updated phylogenetic analyses (Ahlberg & Clack, 1998; Clack et al., 2012; Pardo et al., 2017; Ruta et al., 2003), and new analytical methodologies (Esteve-Altava, 2019; Simões & Pierce, 2021) have revealed previously unrecognized morphological and, presumably, ecological diversity amongst stem tetrapods (but see Anderson et al., 2013). Along with quantitative analyses of performance in locomotor (Ashley-Ross, 1994; Callier et al., 2009; Dickson et al., 2021; King et al., 2011; Molnar et al., 2021; Pierce et al., 2012, 2013; Standen et al., 2014), feeding (Anderson et al., 2011, 2013; Deakin et al., 2022; Dutel et al., 2013, 2015; Fortuny et al., 2015; Heiss et al., 2013; Lautenschlager et al., 2016; Markey & Marshall, 2007; Neenan et al., 2014; Schwarz et al., 2020), and sensory (Clack, 1989, 1994, 1998a, 2002b; MacIver et al., 2017) systems in early tetrapods and extant bracketing taxa, these studies have overturned many earlier ideas of the orderly, step-wise sequence in which "terrestrial" characters were acquired, the functional significance of these innovations, and their role in the invasion of new ecological niches (Clack, 2009; Coates et al., 2008).

One of the most bizarre and enigmatic early tetrapods is *Crassigyrinus scoticus*, known from the Lower Carboniferous (uppermost Visean to lowest Serpukovian) of Scotland (Gradstein et al., 2012). The holotype specimen (NMS G.1859.33.104), consisting of the mediolaterally compressed right side of the upper jaw, was first described by Watson (1929) along with numerous other Carboniferous Scottish 'amphibia' including a right lower

* Corresponding author.
†Author deceased March 26, 2020.

Color versions of one or more of the figures in the article can be found online at www.tandfonline.com/ujvp.

jaw preserved anterior to the adductor fossa and exposed in lateral (labial) view (NHMUK VP R310) that Watson assigned to *Macromerium scoticum* Lydekker, 1890 (Fig. 1A); both specimens are from the same horizon of the Gilmerton Ironstone near Edinburgh. Watson (1929) noted several peculiarities of the holotype, such as the tall 'cheek' below the orbit and posterior displacement of the jaw joint, and reconstructed the skull by reflecting the preserved right side of the upper jaw across the midline, resulting in a broad, flat head (Panchen, 1985:fig. 12). The holotype was re-described by Panchen (1973) who also reexamined NHMUK VP R310 and assigned the latter specimen to *Loxomma*. Panchen (1985) subsequently described the most complete specimen of *C. scoticus*—NHMUK VP R10000 ('Dora') from the Dora Bonebed of Cowdenbeath, Fife—consisting of a nearly complete skull that is dorsoventrally crushed (Fig. 1B) and most of the presacral skeleton. Additional *C. scoticus* material from the Dora Bonebed includes a matching quadrate and articular (NMS G.1975.40.50/51), and a pelvic girdle, hindlimb, and vertebral elements (Panchen & Smithson, 1990) that pertain to separate individuals. In his description of NHMUK VP R10000, Panchen (1985) re-evaluated NHMUK VP R310 and assigned it to *C. scoticus*. Additionally, he identified two specimens from the Gilmerton Ironstone—GSE 4722, a left lower jaw preserved anterior to the adductor fossa exposed in medial (lingual) view and broken into three pieces (Fig. 1C), and NHMUK PV OR30532, the anterior two-thirds of a dorsoventrally crushed skull exposed in palatal view (Fig. 1D)—as pertaining to *C. scoticus*, as well as an unregistered GSE specimen from Gilmerton consisting of the anterior portion of a right lower jaw. Two-dimensional (2D) reconstructions based on information from NMS G.1859.33.104, NHMUK VP R10000, and NHMUK PV OR30532 suggested that the skull of *C. scoticus* was extremely deep in lateral view (Panchen, 1985:fig. 9) but narrow and V-shaped in dorsal and palatal views (Panchen, 1985:figs. 7 and 11). Careful preparation of the dorsal aspect of NHMUK PV OR30532 led to re-descriptions of this specimen by Clack (1996, 1998b) with new reconstructions featuring a shorter, broader snout than previously depicted (Clack, 1998b: fig. 4). A reconstruction of the medial aspect of the lower jaw of *C. scoticus* was presented by Ahlberg and Clack (1998:fig. 16).

A combination of primitive characters and bizarre specializations has resulted in an uncertain phylogenetic position for *C. scoticus*, although recent analyses have placed the taxon within the tetrapod stem group (Ahlberg & Clack, 1998; Clack et al., 2016; Pardo et al., 2017; Ruta et al., 2003). The discovery of a *Crassigyrinus*-like lower jaw (UMZC 2011.9.1) from the upper Tournasian of Scotland and a recently described *Crassigyrinus*-like fibula from the Tournasian locality of Blue Beach in Nova Scotia, Canada may extend the existence of the genus 20 million years into the base of the Carboniferous and greatly increase its geographic range (Clack et al., 2018; Lennie et al., 2020), although it should be noted that both of these specimens are fragmentary. Postcranial remains possibly pertaining to *Crassigyrinus* have also been described from the Visean–Namurian boundary of Greer and Hinton, West Virginia, U.S.A. (Godfrey, 1988). If these specimens do belong to *Crassigyrinus*, they suggest, along with the presence of various primitive characters, that by the middle Carboniferous *Crassigyrinus* was a long-lived relic taxon.

Medical imaging methods, particularly micro-computed tomography (μCT), are increasingly being applied to fossils (Cunningham et al., 2014), including early tetrapods (Arbez et al., 2022; Boisvert et al., 2008; Herbst & Hutchinson, 2019; Pardo et al., 2017; Pierce et al., 2012; Porro et al., 2015a, 2015b; Rawson et al., 2021). More recently, new techniques have been developed to digitally repair damage and deformation in fossil skulls (Lautenschlager, 2016), including early tetrapod skulls (Porro et al., 2015a, 2015b; Rawson et al., 2021). Although the morphology of *C. scoticus* is known from a number of specimens, all are deformed. In this study, we use μCT and visualization software to digitally prepare the skull from four specimens of *C. scoticus* containing upper and lower jaw material. We digitally isolate individual bones, resulting in a revised osteological description that supplements and amends previous work (Ahlberg & Clack, 1998; Clack, 1996, 1998b; Panchen, 1973, 1985; Watson, 1929). Individual skull bones were then manipulated to produce a three-dimensional (3D) digital model of the morphology of the *C. scoticus* skull, which differs substantially from earlier 2D reconstructions (Clack, 1998b; Panchen, 1985; Watson, 1929).

TABLE 1. Computed tomography scanning information for *Crassigyrinus scoticus* specimens.

Specimen	kV	μA	mm/ voxel	Number of slices
NHMUK VP R10000 (anterior half)	210	200	0.1083	1958
NHMUK VP R10000 (posterior half)	210	200	0.1083	1953
NHMUK VP R10000 (anterior postcranial block, containing basioccipital)	200	200	0.0774	2000
NHMUK VP R10000 (two detached portions of skull roof)	200	200	0.0774	1526
GSE 4722 (anterior)	210	240	0.1271	1995
GSE 4722 (middle)	210	240	0.1099	1995
GSE 4722 (posterior)	210	240	0.1099	1687
NHMUK VP R310 (anterior)	210	200	0.1034	1956
NHMUK VP R310 (posterior)	210	200	0.1034	1939
NHMUK PV OR30532	224	340	0.0942	2840

MATERIALS AND METHODS

Three *C. scoticus* specimens—NHMUK VP R10000, NHMUK VP R310, and GSE 4722—were μCT-scanned at the Imaging and Analysis Centre of the Natural History Museum (London, U.K.) while a fourth specimen (NHMUK PV OR30532) was scanned at the University of Bristol Life Sciences Building (Bristol, U.K.). All specimens were scanned on Nikon XT H 225 μCT scanners (Nikon Metrology, Tring, U.K.), producing a total of 10 μCT data sets (Table 1). NHMUK VP 10000 was scanned in four portions: the anterior and posterior halves of the skull, the anterior postcranial block (containing the displaced basioccipital), and two detached portions of the skull roof that were scanned together. NHMUK VP R310 was scanned in two halves, the anterior and posterior portions of the lower jaw. GSE 4722 is preserved in three large pieces—the anterior, middle, and posterior portions of the lower jaw—which were scanned individually. Original CT data for all NHMUK specimens are available on Morphosource (https://www.morphosource.org/projects/000489772); original CT data for the GSE specimen is available directly from the British Geological Survey's National Geoscience Data Centre (https://doi.org/10.5285/79ebcef0-16c6-44dc-afef-4b8c51cd459e).

CT scans were processed using the visualization software Avizo 7.1.1 and 8.0 and Amira 6.7.0 (Thermo Fisher Scientific, Waltham, MA, U.S.A.). Within the Segmentation Editor, density thresholding was used to initially separate bone from matrix; scans were then processed slice-by-slice (interpolating across no more than five slices at a time) to separate individual bones and teeth from each other (Figs. 2, 3, S1, S2, S3). Sutures typically present as low-density areas between bones, although occasionally high-density minerals precipitate within them. Original specimens and photographs were used to confirm the location of sutures and differentiate them from post-mortem damage. Three-dimensional surface models (.surf files) of

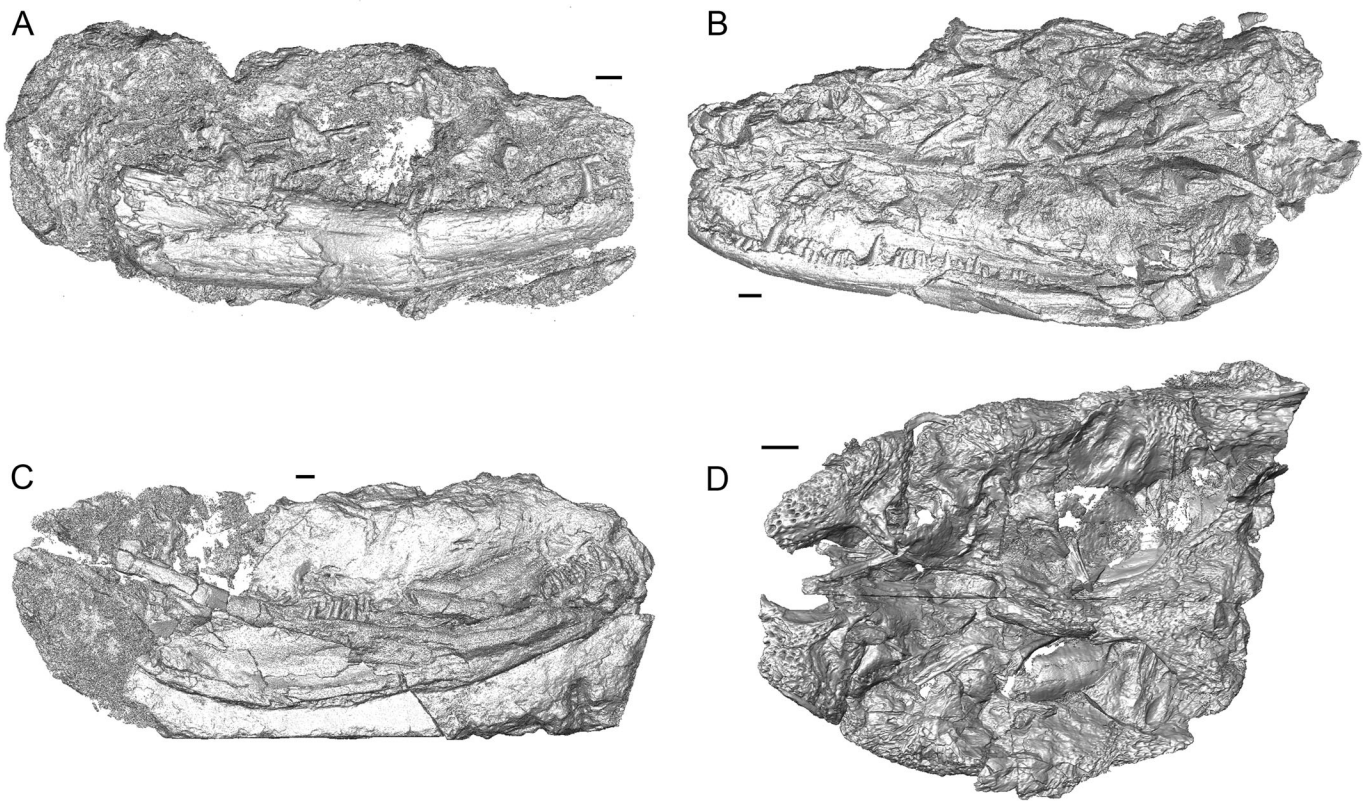

FIGURE 1. Isosurfaces from computed tomography data of *Crassigyrinus scoticus* specimens. **A**, lateral view of NHMUK VP R310; **B**, dorsal view of NHMUK VP R10000 ('Dora'); **C**, medial (lingual) view of GSE 4722; **D**, dorsal view of NHMUK PV OR30532. All scale bars equal 10 mm.

individual bones and teeth were created and could be manipulated in 3D space; the following description is based on these models.

No single specimen of *C. scoticus* preserves a complete skull; however, the four specimens scanned in this study collectively preserve all skull bones. The following limits to the data sets used in the description and 3D reconstruction are noted. NHMUK R10000 preserves a nearly complete skull that has been asymmetrically deformed, resulting in the left side of the upper and lower jaws, as well as the bones of the skull roof, dorsally overlying the right side of the skull, which is visible in ventral view. Some areas of NHMUK VP R10000 (including the frontals, squamosals, and quadratojugals) have been damaged, the skull roof was posteriorly displaced relative to the rest of the cranium, and the basioccipital was detached and preserved with the postcrania (Panchen, 1985). NHMUK PV OR30532 is preserved from the anterior tip of the snout to a point level with the intertemporals. The posterior facial skeleton, posterior skull roof, and most of the braincase are missing, as is the lower jaw. NHMUK VP R310 and GSE 4722 each preserves the anterior two-thirds of the lower jaw but the articular and posterior parts of the surangular, angular, and prearticular are missing; additionally, due to mediolateral crushing, many bones in GSE 4722 are broken. Scan data confirm that no specimen of *C. scoticus* preserves the otic capsules (Panchen, 1985) and it may be that this area was cartilaginous in life.

TABLE 2. Maximum anteroposterior length of selected elements from *Crassigyrinus scoticus* cranial specimens (NHMUK VP R10000 and NHMUK PV OR30532). Only measurements from elements that are represented and nearly complete and undamaged in both cranial specimens are shown.

Specimen	Bone	Side	Length (mm)
R10000	Premaxilla	Left	58.15
OR30532	Premaxilla	Right	81.80
R10000	Maxilla	Left	176.70
R10000	Lacrimal	Left	77.23
OR30532	Lacrimal	Right	92.29
R10000	Nasal	Left	45.68
R10000	Nasal	Right	44.25
OR30532	Nasal	Left	52.35
R10000	Prefrontal	Left	39.89*
R10000	Prefrontal	Right	36.16*
OR30532	Prefrontal	Left	49.09*
OR30533	Prefrontal	Right	46.67*

* Maximum length of the ventral base (that articulates with the lacrimal) of the prefrontal.

Most 3D reconstructions of early tetrapod skulls have been based on individual, well-preserved specimens (Fortuny et al., 2017; Lautenschlager et al., 2016; Porro et al., 2015a), with a few attempts made to reconstruct skulls based on multiple specimens exhibiting moderate deformation (Porro et al., 2015b; Rawson et al., 2021). Reconstruction of the skull of *C. scoticus* was based primarily on bones from the left side and midline of NHMUK VP R10000 with two elements, the palatine and quadrate, taken from the right side due to better preservation. The posterior skull roof (parietals, intertemporals, supratemporals, tabulars, and postparietals) is well-preserved on both sides and all elements are tightly sutured together; it was used in its entirety, thus accounting for slight asymmetries in the skull roof. Additionally, several bones (the left frontal, left vomer, anterior portion of the left pterygoid, and anterior part of the parasphenoid) from NHMUK PV OR30532 were incorporated into the reconstruction after being scaled using elements shared between the two datasets, such as the lacrimal, prefrontal,

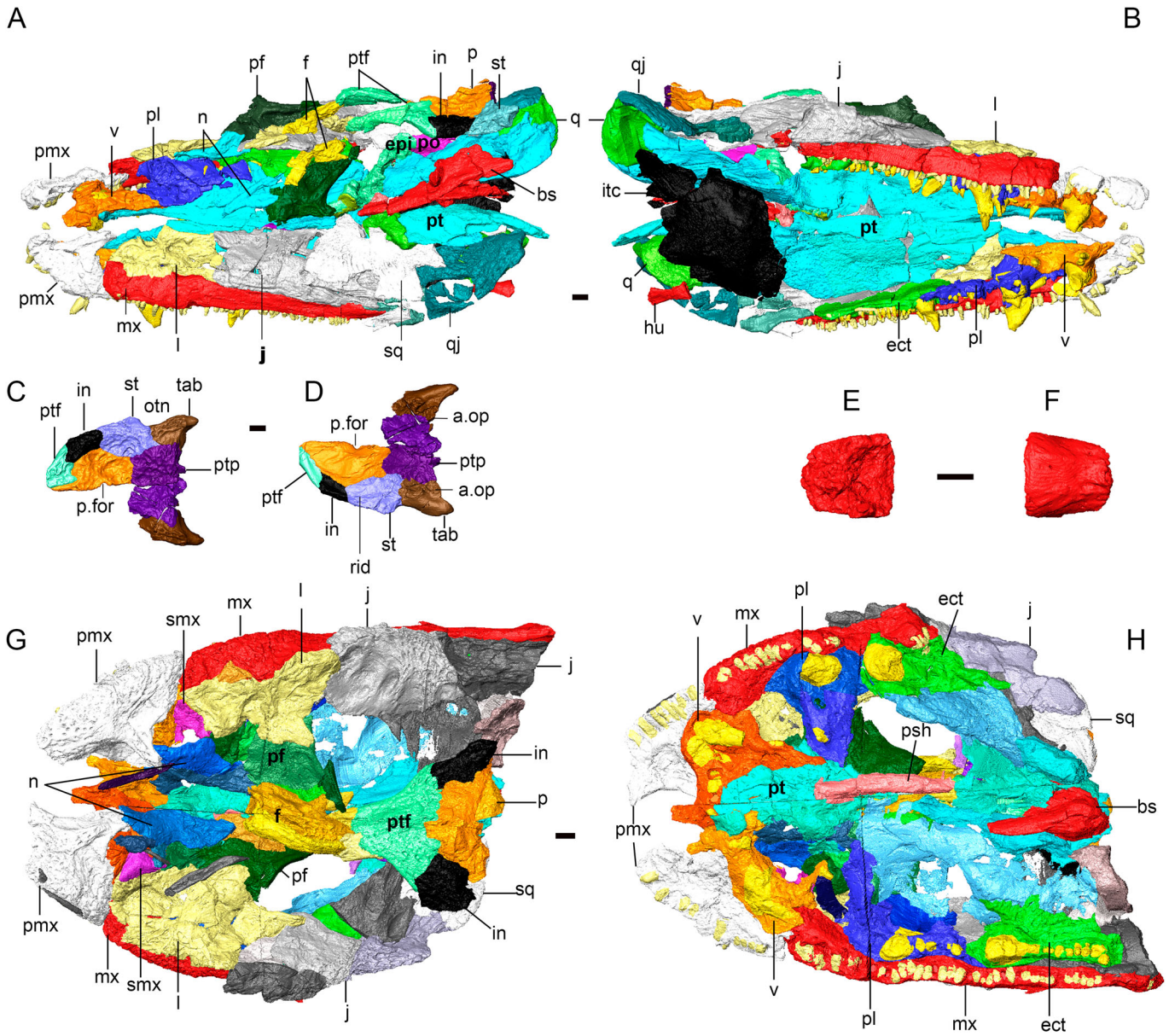

FIGURE 2. Surface models of *Crassigyrinus scoticus* upper jaw material, matrix has been removed. Individual bones are shown in different colors; fragments of the same bone are shown in slightly different shades. **A**, NHMUK VP R10000 cranium in left dorsal view; **B**, NHMUK VP R10000 cranium in right ventral view; **C**, NHMUK VP R10000 detached portion of skull roof in dorsal view; **D**, NHMUK VP R10000 detached portion of skull roof in ventral view; **E**, NHMUK VP R10000 isolated basioccipital in dorsal view, anterior is to the left; **F**, NHMUK VP R10000 isolated basioccipital in ventral view, anterior is to the right; **G**, NHMUK PV OR30532 skull in dorsal view; **H**, NHMUK PV OR30532 skull in ventral view. All scale bars equal 10 mm.

and jugal (Table 2). Comparisons between these shared elements suggest that NHMUK VP R10000 was approximately 82% of the size of the larger NHMUK PV OR30532; this scaling factor was considered when importing bones from NHMUK PV OR30532 that were poorly preserved in NHMUK VP R10000 (see transform matrices in Supplementary Information 3, Supplementary Text). Allometric differences between the specimens may be possible, given the difference in size. However, apart from variations in the direction of overlap (see Discussion), significant morphological variation was not noted between the specimens, and only two bones and portions of two other bones from NHMUK PV OR30532 were incorporated into the model (see Supplementary Information 3, Supplementary Text). Therefore, the addition of these elements is unlikely to have introduced error into the 3D reconstruction. The lower jaw was reconstructed entirely based on bones from the left side of NHMUK VP R10000. With the exception of the skull roof and single median elements, all bones were reflected across midline to create both sides of the cranium.

Using the Transform Editor within Avizo/Amira, the parasphenoid, basisphenoid, and basioccipital were first arranged along the Z axis (taken as the midline); the palatal elements were then assembled around the midline bones so that the palate was initially oriented horizontally, which is often assumed for early tetrapods. The cranium was built upwards by fitting the remaining cranial bones together at well-defined sutural contacts, finishing with the skull roof (Figs. 4, 5, 6, 7, 8, 9). This resulted in an initial 3D reconstruction that contained

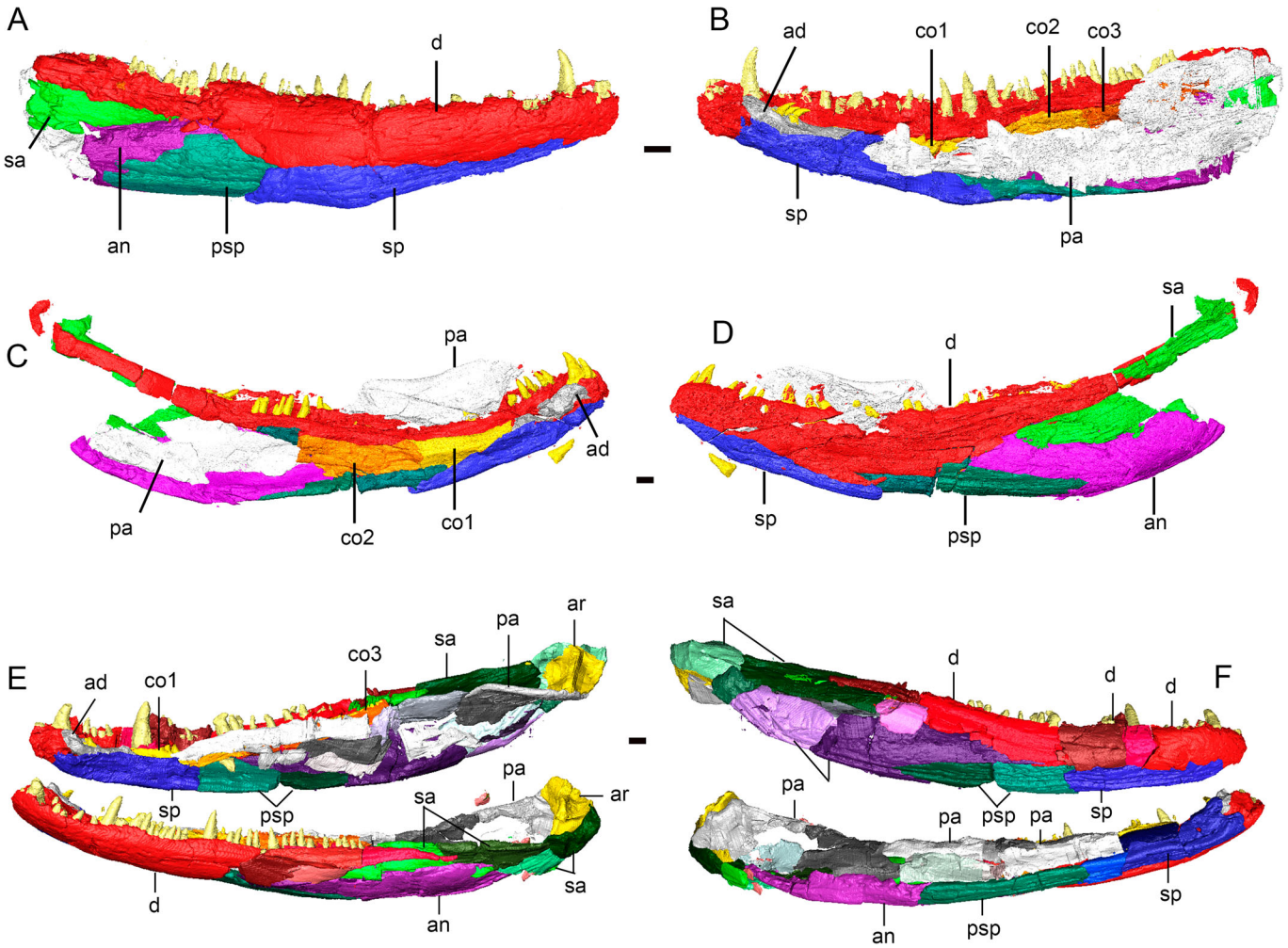

FIGURE 3. Surface models of *Crassigyrinus scoticus* lower jaws, matrix has been removed, individual bones are shown in different colors. **A**, NHMUK VP R310 in lateral view; **B**, NHMUK VP R310 in medial view; **C**, GSE 4722 in medial view; **D**, GSE 4722 in lateral view; **E**, NHMUK VP R10000 lower jaws in left dorsal view; **F**, NHMUK VP R10000 lower jaws in right ventral view. All scale bars equal 10 mm.

several discrepancies, including: a wide midline gap between the pterygoids (not present in either NHMUK VP R10000 or PV OR30532); a gap between the dorsal margins of the squamosal and quadrate ramus of the pterygoid; no contact between quadrate and the quadratojugal (laterally) or pterygoid (medially); the epipterygoid unable to span the vertical distance between the palate and skull roof; and the anterior parasphenoid and anterior pterygoids located at different vertical levels. All of these issues were corrected by moderate dorsal vaulting of the palate (Fig. 7, resulting in an angle of approximately 160° between the 'horizontal' laminae of the left and right pterygoids), requiring shifting of other cranial bones. The intramandibular angle of the reconstructed lower jaws (23.4°, measured from the symphysis to the posterior tips of the surangulars) was determined by precisely aligning the enlarged palatal fangs with their respective fossae in the lower jaws, the adsymphysial teeth with the anterior palatal fossa (see Results below), and fitting together the quadrate and articular at the jaw joint (Fig. 6E, G). Finally, breaks within individual bones were repaired using interpolation; it should be noted that a few bones, particularly the squamosal, quadratojugal, and postorbital, required more extensive reconstruction. 3D models of the reconstructed upper and lower jaws are available for inspection (Supplementary Information 1 and 2). Transformation matrices for all skull bones from the original CT data set to the final 3D reconstructed model are also available (Supplementary Information 3, Supplementary Text). It should be noted that this 3D model represents our best hypothesis of the shape of *C. scoticus* skull based on available specimens, scan resolution, and personal interpretation.

Institutional Abbreviations—**GSE**, Institute of Geological Sciences (British Geological Survey), Edinburgh, U.K.; **NHMUK**, The Natural History Museum, London, U.K.; **NMS**, National Museums of Scotland, Edinburgh, U.K.; **UMZC**, University Museum of Zoology, Cambridge, U.K.

Anatomical Abbreviations—**ad**, adsymphysial; **an**, angular; **a.op**, articulation surface for opisthotic; **apf**, anterior palatal fossa; **ar**, articular; **bo**, basioccipital; **bs**, basisphenoid; **co1**, anterior coronoid; **co2**, middle coronoid; **co3**, posterior coronoid; **d**, dentary; **ect**, ectopterygoid; **en**, external naris; **epi**, epitpterygoid; **f**, frontal; **hu**, humerus; **in**, intertemporal; **ipf**, interpremaxillary fenestra; **ir**, internal naris; **itc**, interclavicle; **j**, jugal; **l**, lacrimal; **maf**, mandibular adductor fossa; **mf**, Meckelian fenestra; **mx**, maxilla; **n**, nasal; **o**, orbit; **otn**, otic notch; **p**, parietal; **pa**, prearticular; **pf**, prefrontal; **p.for**, parietal foramen; **pl**, palatine; **pmx**, premaxilla; **po**, postorbital; **psh**, parasphenoid; **psp**, postsplenial; **pt**, pterygoid; **ptf**, postfrontal;, **ptp**, postparietal; **q**, quadrate; **qj**, quadratojugal; **rid**, ridge; **sa**, surangular; **sf**, subtemporal fossa; **smx**, septomaxilla; **sp**, splenial; **sq**, squamosal; **st**, supratemporal; **tab**, tabular; **v**, vomer.

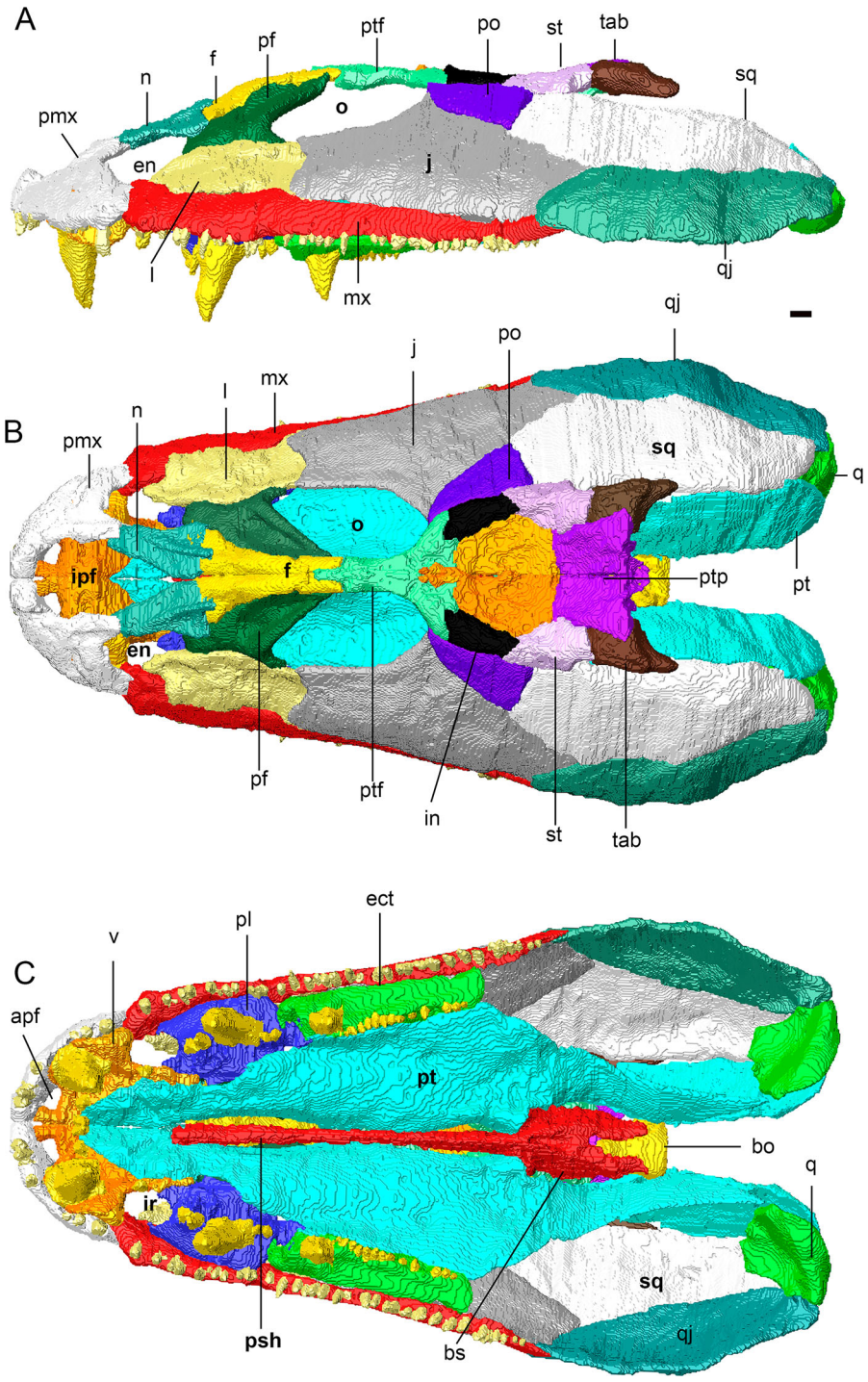

FIGURE 4. 3D reconstruction of the cranium of *Crassigyrinus scoticus*. Individual bones shown in different colors. **A**, left lateral view; **B**, dorsal view; **C**, ventral view. All scale bars equal 10 mm.

RESULTS

Facial Skeleton and Cheek

Two specimens scanned for this study, NHMUK VP R10000 and NHMUK PV OR30532, preserve upper jaw material. NHMUK VP R10000 measures 316 mm from the anterior tip of the left premaxilla to the posterior tip of the left tabular; however, the skull roof has been posteriorly displaced, exaggerating cranial length. NHMUK PV OR30532 measures 314 mm from the anterior tip of the right premaxilla to the broken posterior edge of the right maxilla (maximum preserved length of the specimen). Measurements from selected elements of both skulls are presented in Table 2, demonstrating the larger size of NHMUK PV OR30532.

Premaxilla—The premaxilla of *C. scoticus*, previously described by Panchen (1973, 1985) and Clack (1996, 1998b), is a massive triangular bone with deeply embayed anterodorsal and posterodorsal margins, a ventrally convex alveolar margin, and a long, posterodorsally tapering process (=premaxillary buttress of Clack [1998b]) (Figs. 2, 4, S1A–D). The premaxilla is

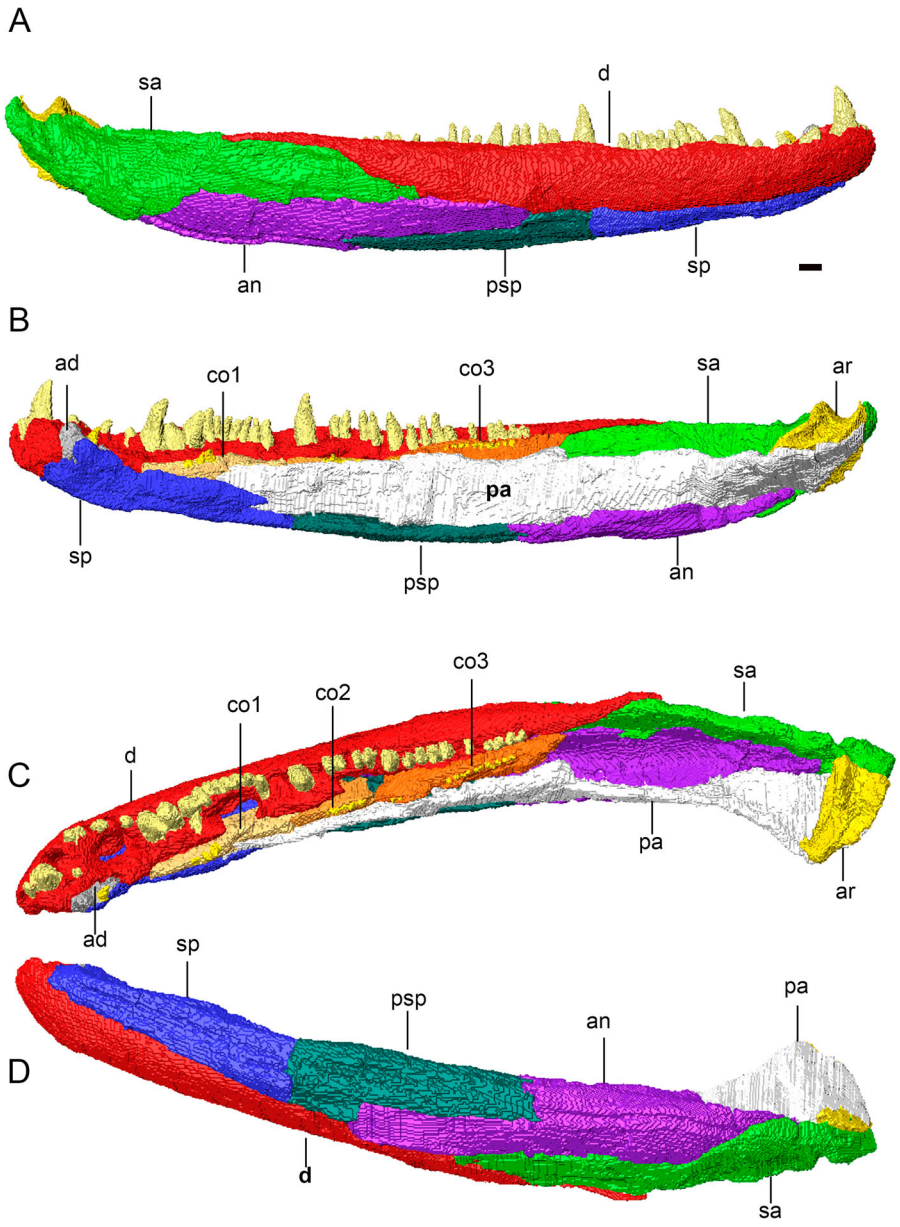

FIGURE 5. 3D reconstruction of the right lower jaw of *Crassigyrinus scoticus*. Individual bones shown in different colors. **A**, right lateral view; **B**, medial view; **C**, dorsal view; **D**, ventral view. All scale bars equal 10 mm.

complete and well-preserved on both sides of NHMUK PV OR30532, and on the left side of NHMUK VP R10000; it is broken on the right side of NHMUK VP R10000. In transverse section, the body of the premaxilla is slightly laterally bowed and is mediolaterally widest at the alveolar margin, narrowing dorsally. There is no medial premaxillary shelf, unlike *Acanthostega* (Porro et al., 2015b). Scans reveal the presence of 10 premaxillary teeth plus four empty alveoli (left) and eight premaxillary teeth plus three empty alveoli (right) in NHMUK VP R10000. There appear to be eight premaxillary teeth and four alveoli (left) and 10 premaxillary teeth plus three alveoli (right) in NHMUK PV OR30532. Therefore, the premaxilla of *C. scoticus* appears to bear a maximum of 14 teeth, higher than the tooth count reported by Panchen (1985) but lower than that reported by Clack (1996, 1998b). The premaxillary teeth are round in cross section and nearly straight in lateral view.

The presumed anterior contact between the premaxillae has opened in both specimens; it appears this was a simple butt joint. The short, stout anterior process demarcates the anterior margin of the unusual interpremaxillary fenestra (=internarial fontanelle of Pardo et al. [2017] and the internasal fontanelle of Lebedev and Clack [1993]). The anterodorsal margin of the premaxilla is strongly embayed and the bone smoothly excavated, forming the lateral margin of the interpremaxillary fenestra, which is bounded posteriorly by the premaxillary buttress. This buttress, which features a strong ridge, anteriorly bounds the smoothly excavated posterodorsal margin of the premaxilla, which forms the anterior margin of the external naris. The tip of the premaxillary buttress is grooved to receive the anterior tip of the nasal. The posterior edge of the premaxilla is laterally overlapped by the rounded anterior margin of the maxilla in an interdigitating suture. The degree of contact between the premaxilla and the lacrimal varies between and within specimens (see Discussion).

The medial aspect of the posterior half of the premaxilla contacts the massive, curving body of the vomer (bearing enlarged

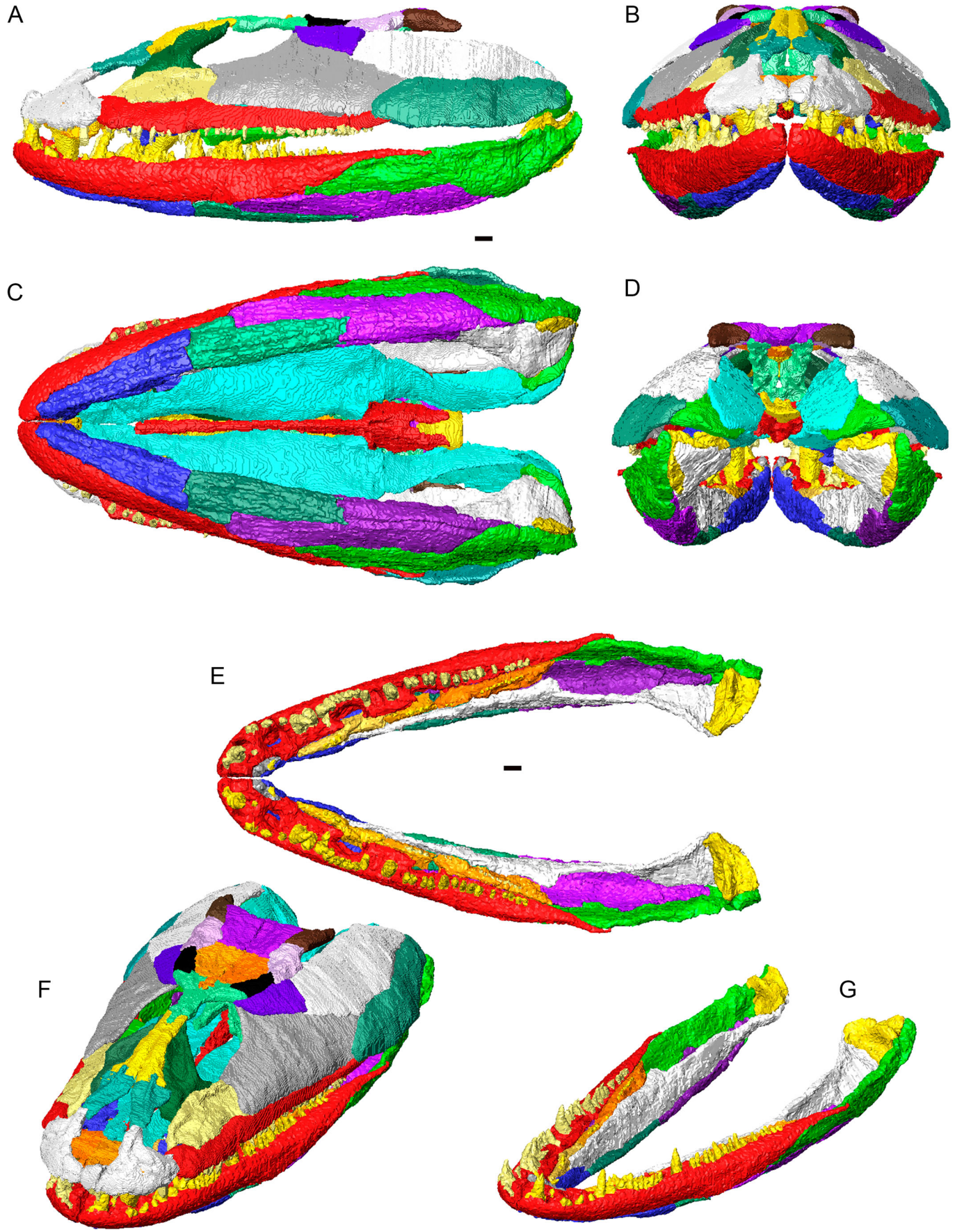

FIGURE 6. 3D reconstruction of the cranium and lower jaws of *Crassigyrinus scoticus* in articulation. Individual bones shown in different colors. **A**, left lateral view; **B**, anterior view; **C**, ventral view; **D**, posterior view; **E**, articulated lower jaws (no cranium) in dorsal view; **F**, cranium and lower jaw in dorsolateral oblique view; **G**, articulated lower jaws in dorsolateral oblique view. All scale bars equal 10 mm, no scale bars for oblique views.

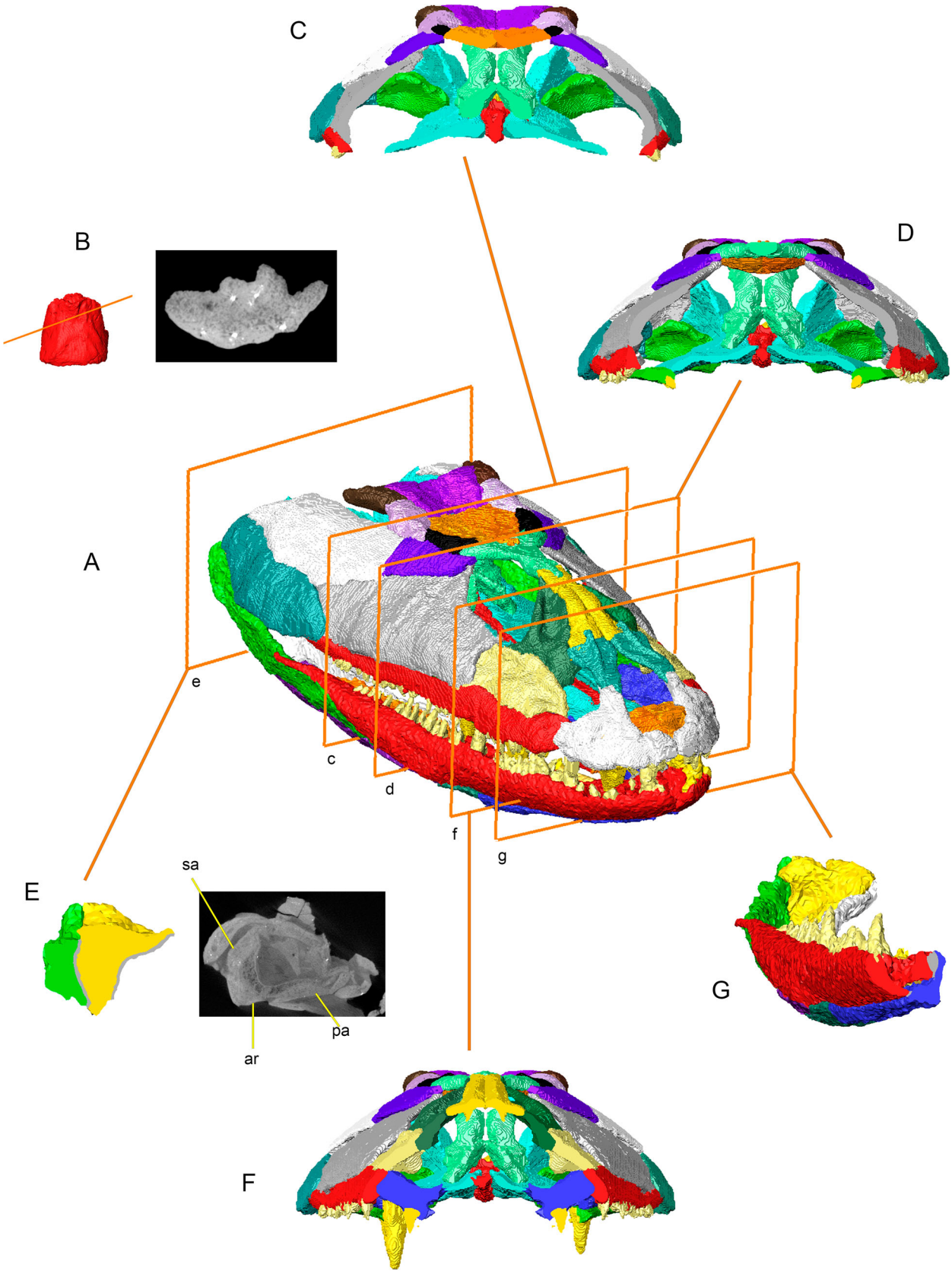

FIGURE 7. Selected cross sections from 3D model of the articulated cranium and lower jaws of *Crassigyrinus scoticus.* Individual bones shown in different colors. Lower case letters in **A** indicate corresponding slices. **A**, 3D model of skull in dorsolateral oblique view; **B**, 3D model of the basioccipital in ventral view (anterior is upwards) with corresponding transverse slice from corresponding original CT data of NHMUK VP R10000 demonstrating bone porosity (slice is not shown in **A** because the basioccipital is internal to the facial and skull roof bones); **C**, transverse slice through reconstructed cranium immediately anterior to the basal articulation; **D**, transverse slice through reconstructed cranium at the approximate midpoint of the main body of the pterygoid; **E**, transverse slice through reconstructed lower jaw showing contact between the surangular (green) and articular (yellow) with transverse slice from the similar region of original CT data of NHMUK VP R10000 demonstrating articular and surrounding contacts; **F**, transverse slice through reconstructed cranium through the palatine; **G**, transverse slice through the anterior end of the reconstructed lower jaw showing cross-sectional geometry of the anterior splenial. Not to scale.

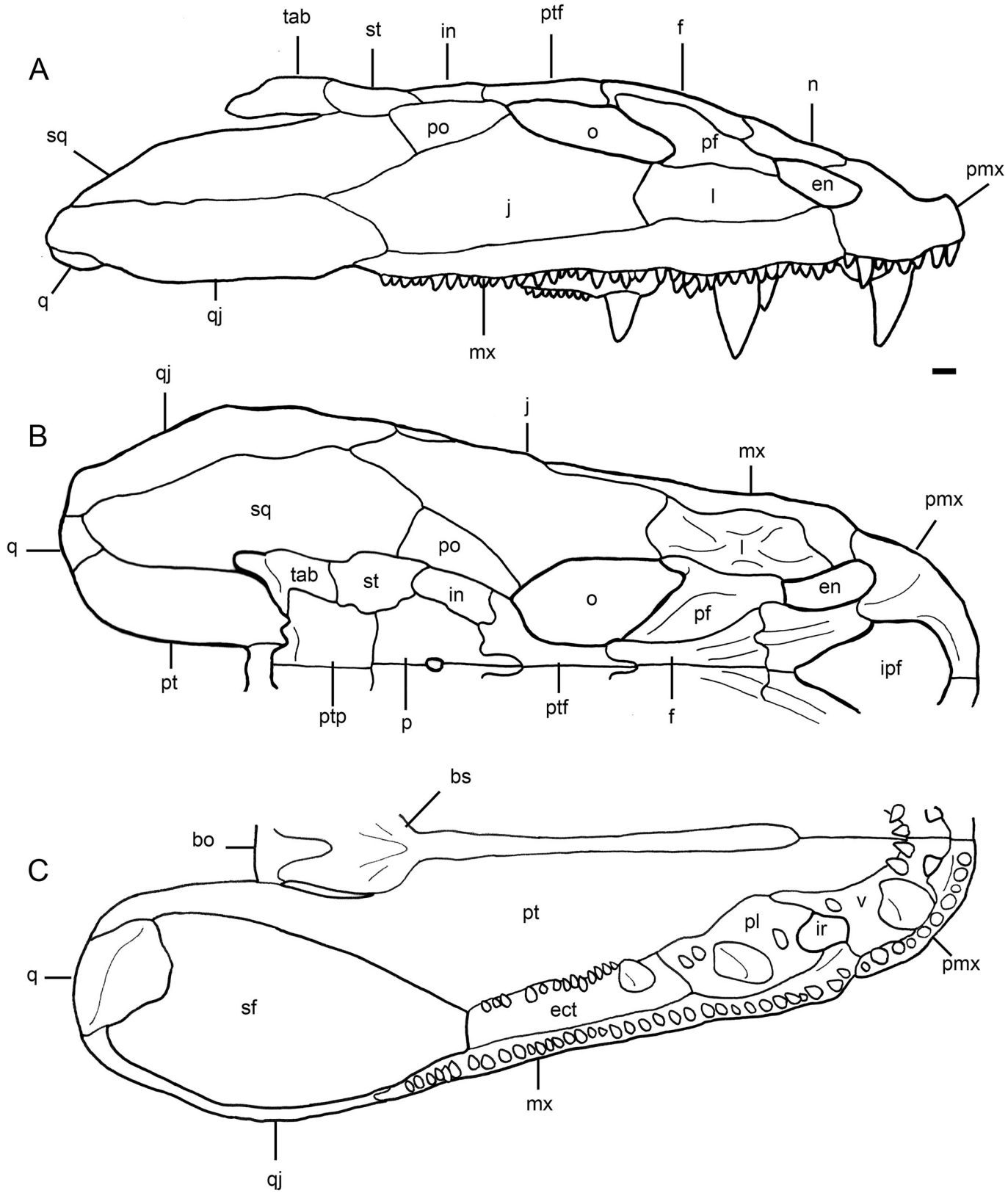

FIGURE 8. Line drawings of the 3D reconstruction of the cranium of *Crassigyrinus scoticus*, clearly showing contacts between bones, dentition, and major skull openings. **A**, right lateral view; **B**, dorsal view (left half of cranium); **C**, ventral view (left half of cranium). Scale bar equals 10 mm.

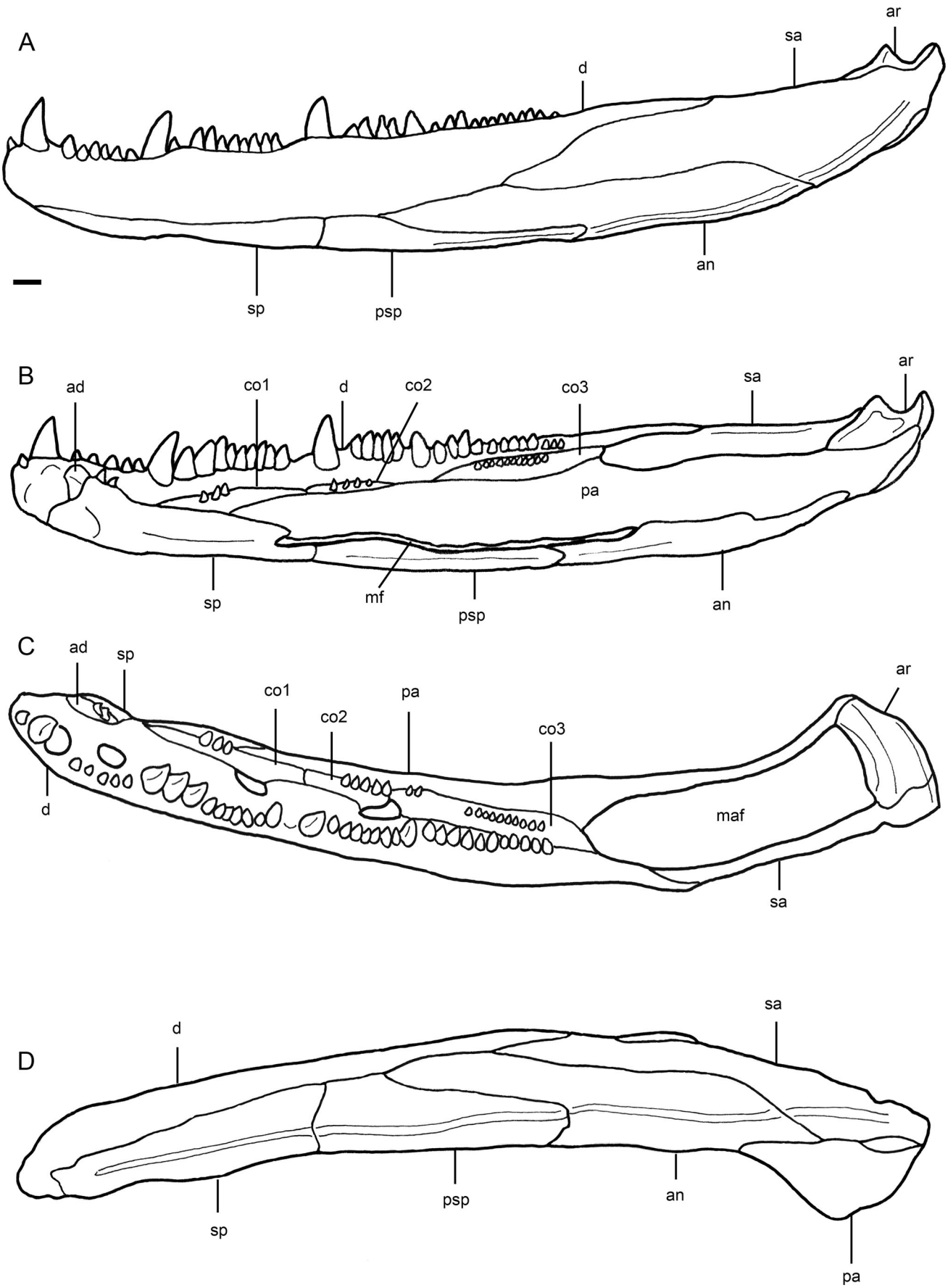

FIGURE 9. Line drawings of the 3D reconstruction of the lower jaw of *Crassigyrinus scoticus*, clearly showing contacts between bones, dentition, and major openings. **A**, lateral view (of left side); **B**, medial view (of right side); **C**, dorsal view of left side; **D**, ventral view of left side. Scale bar equals 10 mm.

fangs, see below) at an expansive, strongly interdigitated contact, as suggested by Clack (1996). Anterior to the vomerine fangs, the premaxilla and vomer separate to form the anterior palatal fossa, which is dorsally confluent with the interpremaxillary fenestra (Clack, 1998b). The premaxilla forms the anterior and lateral margins of the anterior palatal fossa, while the vomer forms the posterior and medial margins (Fig. 4C). The anterior processes of the vomers, preserved in NHMUK PV OR30532 and NHMUK VP R10000, articulate with the premaxillary processes, which are preserved in the holotype (Clack, 1996), in the new 3D reconstruction, as originally suggested by Clack (1996, 1998b).

In both NHMUK VP R10000 and NHMUK PV OR30235, the external surface of the body of the premaxilla (above the tooth row) is densely covered in small openings; these radiate anteriorly and posteriorly from the center of the premaxilla. CT scans demonstrate that these openings lead to short canals within the bone; however, the canals are not connected to each other or to a central canal. Thus, they probably do not represent the main lateral line canal system. Instead, they may mark the positions of superficial neuromasts of the peripheral lateral line system, which is highly variable among extant fish (Mogdans, 2019).

Maxilla—The maxilla is well-preserved on the right side of NHMUK PV OR30532 and on both sides of NHMUK VP R10000 (Figs. 2, S1E–H). The maxilla of *C. scoticus* is an anteroposteriorly elongate but dorsoventrally narrow bone. It is tallest anteriorly and tapers to a point posteriorly in lateral view. In palatal view, the anterior ends of both maxillae in NHMUK PV OR30532 curve and expand medially to contact the premaxillae and vomers. In transverse section, the maxilla is gently laterally convex and is mediolaterally widest at the tooth bases, narrowing dorsally. There is an incipient medial maxillary shelf, which becomes more pronounced posteriorly. CT scans demonstrate that the right maxilla of NHMUK VP R10000 contains 32 teeth and 16 empty alveoli, whereas the left maxilla contains 34 teeth and nine empty alveoli. The nearly complete right maxilla of NHMUK PV OR30532 contains 31 teeth and 12 alveoli. This results in a maximum count of 48 maxillary teeth in *C. scoticus*, substantially more than reported in previous studies (Clack, 1998b; Panchen, 1985). Furthermore, whereas previous reconstructions depict the posterior quarter of the maxilla as being toothless (Clack, 1998b; Panchen, 1985), CT scans demonstrate that the tooth row extended nearly the full length of the maxilla. The anterior half dozen maxillary teeth are the largest; the remaining teeth are smaller and generally uniform in size. The maxillary teeth are gently curved medially and very gently recurved in lateral view.

The anterodorsal tip of the maxilla closely approaches the posteroventral corner of the external naris although its contribution to the naris varies between specimens (see Discussion). The anterior half of the dorsal margin of the maxilla shares a long contact with the lacrimal. Anteriorly, the ventral margin of the lacrimal extensively overlaps the dorsal edge of the maxilla in an interdigitating suture; posteriorly, the contact becomes a rounded butt joint. The posterior half of the dorsal margin of the maxilla contacts the jugal. Anteriorly, the maxilla meets the ventral margin of the jugal in a smooth, rounded butt joint; posteriorly, the maxilla laterally overlaps the jugal. The maxilla terminates as a tapering point that ventrolaterally laps the quadratojugal, excluding the jugal from the ventral margin of the skull (Panchen, 1973, 1985) and bounding the anterolateral corner of the subtemporal fossa.

The maxilla forms the lateral wall of the choana in palatal view (Figs. 4C, S1F, H). The extent to which the maxilla contacts the vomer varies between specimens (see Discussion). The lateral aspects of the palatine and ectopterygoid make anteroposteriorly long and dorsoventrally broad interdigitated contacts with the medial aspect of the maxilla, fitting above the medial maxillary shelf. These contacts are very strong and undisturbed on both sides of NHMUK VP R10000 and on the right of NHMUK PV OR30532.

Panchen (1973) described irregular ornamentation on the external surface of the anterior maxilla of the holotype, becoming longitudinal grooves posteriorly. This pattern can be observed in both NHMUK VP R10000 (particularly on the right side) and NHMUK PV OR30532. These openings appear to radiate from an area of the maxilla below the approximate anteroposterior midpoint of the lacrimal; thus, anterior to this point the pores open towards the premaxilla and posterior to this point the openings face posteriorly, elongating into grooves in the posterior half of the maxilla. Unlike the premaxillary openings, CT scans of both sides of NHMUK VP R10000 demonstrate that these openings join a longitudinal canal that extends the length of the maxilla immediately above the tooth implantation zone. This canal cannot be clearly visualized in NHMUK PV OR30532 due to crushing.

Septomaxilla—Both sides of NHMUK PV OR30532 feature a triangular element at the posterior margin of the external nares, which is identified as the septomaxilla, sometimes called the lateral rostral (Panchen 1973, 1985; Clack, 1998b) (Fig. 2G). The anterior and lateral margins of the septomaxilla are straight while the anteromedial margin is embayed. The septomaxilla lies dorsal to vomers and immediately anterior to the lacrimal but does not appear to articulate with any of the surrounding elements. These bones are also present in the type specimen but are missing in NHMUK VP R10000 (Panchen, 1973, 1985; Clack, 1998b).

Lacrimal—The lacrimals are present on both sides of NHMUK VP R10000 and NHMUK PV OR30532, with the left lacrimal being better preserved in both specimens (Figs. 2, 4, S2A–D). The lacrimal forms the posterior margin of the external naris; its contribution to the margin of the orbit varies between specimens (see Discussion). The heavy sculpting of the lacrimal is identical in all described *C. scoticus* specimens (Panchen, 1973; Clack, 1998b). Four strong ridges radiate from a central eminence, forming an X shape on the lateral aspect of the lacrimal. These ridges demarcate three sulci located anterior, dorsal, and posterior to the central eminence; the ventral portion of the lacrimal is laterally convex. The most pronounced ridge arches anterodorsally and borders the posterior margin of the external naris. The lacrimal is sinuous in transverse section, reflecting its complex surface ornamentation. Anteriorly, the lacrimal is mediolaterally widest dorsally and thins ventrally; posteriorly, the dorsal and ventral margins of the lacrimal are thickened.

The middle third of the dorsal margin of the lacrimal contacts the prefrontal; this contact is preserved in NHMUK PV OR30532 and the holotype. CT scans demonstrate that the prefrontal extensively underlaps the lacrimal as reported by Clack (1998b) with deep interdigitations. The lacrimal and jugal meet in an extensive overlapping contact without interdigitations, although the direction of overlap varies between specimens (see Discussion). The ventromedial margin of the lacrimal contacts the dorsolateral aspect of the palatine. Anteriorly, this contact is broad and weakly interdigitated; posteriorly, the contact becomes narrow and interdigitated. Additionally, the medial surfaces of both lacrimals in NHMUK VP R10000 and the right lacrimal of NHMUK PV OR30532 feature a strong, spike-like medial projection (deep to the central eminence on the lateral surface). This spike dorsally overlaps the palatine at the level of the enlarged fang. Contact between the ventral margin of the lacrimal and the ectopterygoid varies between specimens (see Discussion).

Panchen (1973) described pores and a sulcus (continuous with the sulcus on the jugal) marking the course of the infraorbital lateral line canal on the external surface of the lacrimal. Both

lacrimals of NHMUK VP R10000 and NHMUK PV OR30532 feature troughs ventral to the ridges radiating from the central eminence; additionally, the left lacrimals of both specimens preserve numerous pores dorsal to the lacrimal-maxilla contact. CT scans demonstrate these small pores lead into the bone's interior; the right lacrimal of NHMUK VP R10000 preserves several larger internal canals connected to the external pores, although these are not as continuous as those present in the maxillae.

Jugal—The pentagonal jugal is the major bone of the cheek and forms the posterior and most of the ventral margins of the orbit (Figs. 2, 4, S2 E, F). Only the left jugal of NHMUK VP R10000 is complete and undistorted; the right jugal of NHMUK VP R10000 has been folded and broken by deformation. The jugals are largely complete in NHMUK PV OR30532 but both sides have broken into multiple pieces. In transverse section, the jugal is strongly laterally bowed with a thickened ventral margin that is medially expanded, forming a small shelf. Posteriorly, the jugal tapers to a point lying between the squamosal and quadratojugal. The jugal-squamosal contact is preserved on the left sides of both NHMUK VP R10000 and NHMUK PV OR30532. CT scans demonstrate that the squamosal laterally and dorsally overlaps the jugal in an extensive scarf contact with no visible interdigitations. The overlapping contact between the jugal and quadratojugal varies between specimens (see Discussion). The postorbital has separated from the jugal on both sides of NHMUK VP R10000 and NHMUK PV OR30532, suggesting this may have been a weak contact. Preparation of the type specimen revealed that the postorbital broadly overlaps the jugal externally with no interdigitations (Clack, 1998b). CT scans reveal that the medial shelf of the jugal dorsally overlaps the dorsolateral margin of the ectopterygoid in a strong, interdigitated suture in both specimens. Whether the jugal contacts the palatine varies between specimens (see Discussion).

The jugal is one of the most heavily ornamented bones of the skull. A horizontal sulcus, first noted by Panchen (1973), parallels the jugal-maxilla suture; this sulcus is more prominent on the anterior half of the jugal, particularly in the holotype, on the left side of NHMUK VP R10000, and on the right side of NHMUK PV OR30532. Numerous pores open above and below as well as within this sulcus. CT scans of left jugal of NMMUK VP R10000 reveal a longitudinal canal through the jugal immediately dorsal to the sulcus; many (but not all) of the pores connect to this canal, supporting the suggestion that at least some of these openings formed part of the infraorbital lateral line system (Panchen, 1973). Blind-ended canals could either represent parts of the peripheral lateral line system or ornamentation (Clack, 1998b). Posterior to the orbit, the main sulcus turns dorsally and courses towards the postorbital. Between this vertical leg and the anterior horizontal sulcus, a variable number of bony ridges radiate anterodorsally; these ridges surround concave areas on the anterodorsal portion of the jugal and are peppered with blind-ended pores. A number of pores occur within and immediately around the vertical sulcus; dorsally, approaching the contact with the postorbital, these pores elongate into grooves and striations. CT scans of the right jugal of NHMUK PV OR30532, in which the vertical sulcus is well-preserved, demonstrate that the pores within the groove penetrate deep into the jugal, although no continuous canal can be discerned. Many of the surrounding pores and grooves appear to be blind-ended. Posterior to the vertical leg, the horizontal sulcus appears to bifurcate into two short sulci, both of which contain pores: one continues to parallel the jugal-maxilla suture, the other turns posterodorsally. The extensive area between and posterior to these sulci contains a number of elongate, posteriorly directed pores.

Squamosal—NHMUK PV OR30532 preserves only fragments of the squamosals. The anteroventral margin of the right squamosal of NHMUK VP R10000 is missing; CT scans demonstrate that the dorsal portion is well-preserved deep to the displaced skull roof. The ventral margin of the left squamosal of NHMUK VP R10000 (Figs. 2A, S2G, H) is missing several fragments; this bone forms much of the element incorrectly identified as the jugal by Panchen (1985). Deformation of NHMUK VP R10000 has exaggerated the degree of overlap between the squamosal, jugal, and quadratojugal, and has broken and displaced two large fragments of the squamosal from its dorsal margin; this breakage is repaired in the new reconstruction (Fig. 4).

The squamosal is a large bone, with much of its dorsal edge forming the posterior margin of the upper jaw. The postorbital laterally overlaps the dorsal margin of the squamosal in an extensive contact without interdigitations as reported in the type (Clack, 1998b). The ventral margin of the squamosal laterally overlaps the dorsal margin of the quadratojugal. In transverse section, the squamosal is laterally bowed, the dorsal margin is thickened, and the bone tapers ventrally. The dorsal margin is inturned; anteriorly, this inflection is flattened to support the bones of the skull roof. The skull roof is not preserved in the type and is displaced relative to the cheek bones in both NHMUK VP R10000 and NHMUK PV OR30532; however, the morphology of the ventral aspect of the supratemporal suggests it met the flattened dorsal margin of the squamosal in an undulating butt joint without interdigitations. NHMUK PV OR30532 suggests there was a short butt contact between the squamosal and intertemporal although this may be a displacement artifact. The morphology of the articular surfaces between the squamosal and skull roof does not support the presence of a kinetic joint at this contact (contra Panchen, 1985). In both the type and NHMUK VP R10000, the medial aspect of the inturned dorsal edge of the squamosal is thickened, and bears a shallow groove with interdigitations (Clack, 1998b), indicating the contact between the squamosal and vertical process of the pterygoid, although only a short section of this contact is preserved intact on the right side of NHMUK VP R10000. The medial surface of the squamosal meets the apex of the quadrate in a limited contact.

The ornamentation of the squamosal is best preserved in the type, and consists of pits and grooves that radiate ventrally and posteroventrally from its contacts with the skull roof. CT scans of the left squamosal of NHMUK VP R10000 demonstrate that many of these pits connect to canals within the bone. One such canal is particularly persistent, first appearing near the anteroposterior midpoint of the squamosal and coursing posterodorsally through the bone, terminating at a break. Thus, it is likely that at least some of the ornamentation of the squamosal is associated with the lateral line system, although there are no distinct sulci as in the jugal.

Quadratojugal—The quadratojugal (Figs. 2, 4, S2I) is a large bone forming the posteroventral corner of the skull. It is oval-shaped, being tallest in its midsection, tapering to a point anteriorly and a rounded margin posteriorly. The quadratojugal is well-preserved in the type and missing in NHMUK PV OR30532. The anterior portion of the right quadratojugal of NHMUK VP R10000 has been twisted and broken, and much of its ventral margin is missing; the left quadratojugal is nearly complete, being perforated by several small holes. In transverse section, the anterior part of the quadratojugal is mediolaterally thin and nearly vertical; posteriorly, the bone thickens and is strongly laterally bowed. The ventral edge of the quadratojugal forms most of the lateral margin of the subtemporal fossa. The medial aspect of the quadratojugal meets the lateral aspect of the quadrate in a dorsoventrally broad, undulating contact.

The external surface of the quadratojugal features pits and grooves that radiate from the posterior corner, being elongated

particularly along the ventral border of the element. CT scans of the left quadratojugal of NHMUK VP R10000 reveal several large longitudinal canals within the bones that connect to external pores; these merge posteriorly and exit as a single large pore on the lateral aspect of the quadratojugal near its posterior margin (Figs. 2A, S2I), suggesting the lateral line canal system extended onto the bone.

Preopercular—The presence of a preopercular in *C. scoticus* is contested. Panchen (1973) identified and illustrated the preopercular as forming part of the posterodorsal margin of the skull in NMS G.1859.33.1, suturing with the dorsal margins of the squamosal and quadratojugal. Panchen (1985) later identified the preopercular in NHMUK VP R10000 as an isolated element overlying the left jugal (the latter now identified as the left squamosal, see above). However, in her re-analysis of NMS G.1859.33.1, Clack (1998b) found no evidence of a preopercular on either the internal or external surfaces.

The element identified as the preopercular by Panchen (1985) in NHMUK VP R10000 has an unusual morphology (Fig. S9J–L): it is anteroposteriorly elongate with a U-shaped cross-section. The anterior end flattens into an expanded plate. Along with a lack of any obvious articular surfaces along the dorsal margins of the quadratojugal and squamosal, it is highly unlikely that this element represents the preopercular or that a preopercular occurred in *C. scoticus*. The element remains unidentified but most likely represents part of the braincase.

Quadrate—Both quadrates of NHMUK VP R10000 are present and complete, with the right element articulated to the lower jaw (Figs. 2A, B, S3); a right quadrate is preserved in the type and a left quadrate in NMS G.1975.40.50/51. In ventral view, the quadrate is tear-drop shaped with a rounded posterior margin and tapered anterior end. In lateral view, it is shaped like an inclined crescent. The thickened posteroventral margin meets the articular of the lower jaw to form the complexly shaped jaw joint, which is posteriorly convex, mediolaterally expanded, and anteroposteriorly short, although it widens slightly laterally. There is only a single condyle, which is 'U'-shaped in ventral view as described by Panchen (1985); the joint surface is anteroposteriorly convex but mediolaterally concave, or saddle-shaped. As noted by Panchen (1985) the joint surface has a sharply defined posterior rim that stands clear of the posterior aspect of the quadrate when viewed from behind. The anterior aspect of the quadrate (dorsal to the joint surface) is deeply excavated. The dorsolateral aspect of the quadrate broadly contacts the medial aspect of the quadratojugal while the dorsomedial surface is extensively overlapped by the quadrate ramus of the pterygoid. The apex of the quadrate meets the medial surface of the squamosal in a short contact. As preserved in NHMUK VP R10000, the epipterygoid is located far anterior to the quadrate; it is unclear why Panchen (1985) described the epipterygoid contacting the quadrate and contributing to the jaw joint as neither of these appears likely. It is possible that Panchen (1985) was referring to the quadrate wing of the pterygoid.

Skull Roof

Nasal—Both nasals are preserved in NHMUK VP R10000 and NHMUK PV OR30532 (Figs. 2, 4, S4), with individual elements sustaining varying degrees of damage; additionally, the right nasal is preserved in the type (Clack, 1998b; Panchen, 1973). Panchen (1985:fig. 3) identified a pair of isolated elements near the right anterior end of NHMUK VP R10000 as the nasal and frontal; CT scans demonstrate that these elements are in fact the dorsal surfaces of the vomer (Clack, 1998b) and palatine, respectively. Clack (1998b) first suggested that the posteriorly displaced elements identified by Panchen (1973, 1985) as the anterior tectals are, in fact, the nasals, and that anterior tectals are absent in *C. scoticus*. The articulated nasals preserved in NHMUK PV OR30532 and CT scans justify this conclusion.

The nasal has a distinctive and complex shape. It is angled in transverse section with horizontal lamina roofing the snout; medially, this horizontal lamina joins a second lamina, which is ventromedially inclined. In dorsal view, the horizontal lamina has anterior, posterior and lateral processes. The medial margin of the horizontal lamina is smoothly curved and bears a strong ridge marking the junction with the vertical lamina; this ridge is continuous with ridges on the premaxillary buttress anteriorly and the frontals posteriorly. The area between these ridges, where the nasals met at the midline, is anteriorly continuous with the interpremaxillary fenestra and posteriorly continuous with the midline groove of the frontals. The anterolateral border of the horizontal lamina, which forms the posteromedial margin of the external naris, is also thickened, and the dorsal aspect of the nasal between these ridges is depressed. The anterior and posterior processes of the horizontal lamina taper to points; the rounded lateral process has a smooth anterior margin and an embayed posterior margin. The vertical lamina of every preserved nasal is damaged due to dorsoventral compression; it is best preserved on the right side of NHMUK VP R10000 and the left side of NHMUK PV OR30532, and appears to have an undulating ventral margin. The medial margin of the anterior process of the horizontal lamina and the anterior half of the vertical lamina posteriorly bound interpremaxillary fenestra.

The anterior tip of the nasal inserts onto a groove on the posterior tip of the premaxillary buttress, dorsally lapping the premaxilla. The nasal-frontal contact is best preserved on the left side of NHMUK PV OR30532 in which the posterior process of the nasal dorsally overlaps the anterior margin of the frontal in an interdigitated contact. The rounded lateral process dorsally overlaps the anteromedial edge of the prefrontal in a smooth scarf joint. The tip of the lateral process of the nasal closely approaches but does not contact the lacrimal on both sides of NHMUK PV OR30532, suggesting a small internal contribution of the prefrontal to the external naris as inferred by Clack (1998b). Presumably, the posterior half of the vertical lamina of the nasal met its opposite at the midline in a contact that is not preserved in any specimen. Also uncertain is whether the ventral margin of the vertical lamina may have contacted the dorsal aspects of the palatal bones. It contacts the vomers in both the type and NHMUK PV OR30532, however, this may be due to compression. Regardless, it is likely that, due to the inclination of these vertical laminae, the midline contact between the nasals was depressed into a groove continuous with that between the frontals.

Prefrontal—The prefrontal (Fig. S5A–D) is well-preserved in the type, on both sides of NHMUK VP R10000, and on the left side of NHMUK PV OR30532; it is broken on the right side of the latter specimen. It is a curved, triangular bone with its apex directed posterodorsally and has medial, lateral, and anterolateral margins. In lateral view, a thickened ridge along the lateral edge of the prefrontal forms the anterodorsal margin of the orbit. At its anteroventral end, this ridge turns sharply posteriorly, producing a distinct tab that formed the anteroventral corner of the orbit. CT scans show that the prefrontal thins medial to the orbital ridge and is dorsally overlapped by the lateral margin of the frontal in a curving scarf joint with faint interdigitations. The prefrontal thickens anteriorly, terminating in a robust base forming the anterolateral margin. This margin is exposed on both sides of NHMUK VP R10000 (Fig. 2A) and bears a series of deep ridges; CT scans of NHMUK PV OR30532 reveal that these are large-scale interdigitations in the extensive scarf joint between the prefrontal and overlapping lacrimal. There is no contact between the prefrontal and jugal on either side of NHMUK PV OR30532, and this region is disarticulated in NHMUK VP R10000; however, there appears to be a

point contact between these bones in the type that excludes the lacrimal from the orbital margin (Clack, 1998b; Panchen, 1973, 1985). Scans demonstrate that the posterior tips of the prefrontals closely approach but do not contact the postfrontals in both NHMUK VP R10000 and NHMUK PV OR30532, unlike the condition illustrated by Panchen (1985) and suggested by Clack (1998b); instead, the pre- and postfrontals are separated by a short section of the frontal.

Frontal—The frontal is an anteroposteriorly elongate and mediolaterally narrow bone with rounded anterior and posterior margins that is dorsally arched in lateral view and makes a small contribution to the orbital margin between the pre- and postfrontals (Figs. 2, 4, S5E, F). The frontals are preserved on both sides of both NHMUK VP R10000 and NHMUK PV OR30532 but are damaged to varying degrees. In transverse section, there is a strong ridge in the center of the bone; the frontal abruptly thins in height both medially and laterally. The medial lamina is short and contacts the opposite frontal at a midline butt joint. Together, the medial laminae of the frontals form a midline groove bounded by longitudinal ridges as described by Clack (1998b); the groove is continuous with the midline depression between the nasals (see above). The lateral lamina is short in the middle of the frontal but expands at the anterior and posterior ends of the bone to contact surrounding elements. Laterally, the frontal overlaps the prefrontal and the posterior process of the nasal overlaps the frontal on the left side of NHMUK PV OR30532, with weak interdigitations visible. Posteriorly, the anterior margin of the postfrontal dorsally overlaps the posterior margin of the frontal in a very tight contact (no interdigitations can be discerned), preventing any contact between the frontals and parietals (Clack, 1998b).

Postfrontal—The postfrontal and its surrounding contacts are well-preserved on both sides of NHMUK PV OR30532, and on the left side of NHMUK VP R10000 (Figs. 2, 4, S6). It is broken on the right side of NHMUK VP R10000. A sliver of bone adjacent to the left postfrontal of NHMUK VP R10000, which was identified as the squamosal by Panchen (1985), represents the anterior part of the right postfrontal. The postfrontal is triangular in dorsal view with its apex directed anteriorly and is dorsally arched in lateral view. Scans reveal it is dorsoventrally thickest laterally and anteriorly, thinning medially and posteriorly. The thickened lateral edge forms most of the dorsal orbital margin. The medial margin is straight and drawn up into a ridge, which is not as strongly developed as the longitudinal ridge of the frontal and flattens posteriorly. The postfrontals meet at the midline in a tight, undulating butt joint. The postfrontal increases in mediolateral width posteriorly and has a distinct tri-lobed posterior margin that broadly overlaps the anterior margin of the parietal in a tight, interdigitated suture. Posterolaterally, the intertemporal dorsally and laterally overlaps the postfrontal in a very tight, strongly interdigitated contact. The dorsal surface of the postfrontal is heavily ornamented with numerous pits whereas its ventral surface is convex and smooth.

Postorbital—The postorbital is only clearly exposed in the type specimen (Clack, 1998b; Panchen, 1973) but scans suggest that it is likely to be preserved in both NHMUK VP R10000 (Fig. 2A) and NHMUK PV OR30532. Based on size, shape, and position, a small element largely hidden from external view by the overlapping left postfrontal and intertemporal—which is unlabeled in Panchen's (1985) illustrations—almost certainly represents the left postorbital of NHMUK VP R10000. Similarly, CT scans reveal a small element deep to the left frontal and postfrontal of NHMUK PV OR30532 that is probably the left postorbital. In both specimens the suspected postorbital is similar in size to the intertemporal; they are both mediolaterally thin and gently laterally bowed in transverse section. The type specimen demonstrates that the postorbital externally overlapped both the jugal and squamosal without interdigitations (Clack, 1998b), and that its anterior margin contributed to the posterior edge of the orbit. Its thickened dorsal margin was presumably overlapped by the lateral edge of the intertemporal, with a possible short contact with the postfrontal; the disruption of these sutures in NHMUK VP R10000 and NHMUK PV OR30532 suggest this was a weak contact. The holotype preserves elongated vertical pits and grooves on the external surface, continuous with the ornamentation on the dorsal jugal.

Parietal—The parietal is complete on both sides of NHMUK VP R10000; the anterior halves of both parietals are preserved in NHMUK PV OR30532 (Figs. 2A, C, S6). The parietal is an irregularly shaped bone forming the center of the skull roof. In transverse section, it is ventrally convex with a nearly uniform dorsoventral thickness. The lateral margin of the parietal contacts three marginal skull bones: the postfrontal (anterolaterally), the intertemporal (laterally), and the supratemporal (posterolaterally). The postfrontal and intertemporal overlap the lateral margin of the parietal in strongly interdigitated contacts. The postfrontal-parietal overlap is particularly extensive, with an elongate medial prong of the parietal inserting between the postfrontals on both sides of the skull in NHMUK VP R10000 (Fig. 2C). This prong is present but reduced in NHMUK PV OR30532. The posterolateral margin of the parietal meets the anteromedial margin of the supratemporal in an interdigitated contact, and its posterior margin meets the anterior edge of the postparietal in a strongly interdigitated suture. The parietal foramen forms a circular opening surrounded by a raised lip between the parietals in NHMUK VP R10000 (Fig. 2C); on the ventral aspect of the parietal, the foramen is situated on a deep circular depression surrounded by strong ridges as described by Panchen (1985) (Fig. 2D). Only the anterior margin of the foramen is preserved in NHMUK PV OR30532; however, CT scans demonstrate the surrounding depression bordered by ridges on the ventral aspect. The midline contact between the parietals is a vertical contact with some interdigitations. The parietal, along with other skull roof bones (the intertemporal, supratemporal, and postparietal) features a surface ornamentation of irregular pits and ridges (Figs. 2C, S6A, D).

Intertemporal—The small, square-shaped intertemporal forms the lateral margin of the skull roof between the postfrontal and supratemporal (Figs. 2C, D, 4, S6). The bone is preserved on both sides of NHMUK VP R10000 and NHMUK PV OR30532, although both intertemporals lack their posterior margins in the latter specimen. The posteriorly convex posterior margin of the intertemporal dorsally overlaps the anterior edge of the supratemporal in a very tight, interdigitated suture. The intertemporal is mildly dorsally arched in transverse section. The dorsal surface is sculpted and the ventral surface is smooth and dorsally concave. Laterally, this concavity is bounded by a curved ridge that parallels the lateral margin of the intertemporal and continues onto the ventral aspect of the supratemporal (Figs. 2D, S6B). Lateral to this ridge, the ventral aspect of the lateral margin of the intertemporal bears an anteroposteriorly elongate facet, presumably for the articulation of the postorbital.

Supratemporal—The supratemporal is a subcircular bone preserved on both sides of NHMUK VP R10000 although the left element is broken (Figs. 2C, D, S6A–C). In transverse section, the supratemporal is dorsoventrally thickest at its midsection, tapering gently medially and laterally. This cross-sectional morphology is due to a prominent ridge on the ventral aspect of the supratemporal. Anteriorly, there is a single ridge that continues onto the ventral aspect of the intertemporal. The ridge divides at the anteroposterior midpoint of the supratemporal; its medial branch is short and curves posteromedially across the supratemporal, laterally bounding a concavity that continues

anteriorly onto the ventral aspect of the intertemporal. The lateral branch parallels the lateral margin of the supratemporal, continues onto the ventral aspect of the tabular, and borders an anteroposteriorly elongate, oval facet that tapers anteriorly and marks the articulation between the supratemporal and squamosal (Figs. 2D, S6B). Panchen (1985) suggested that this contact, as well as the anteriorly continuous intertemporal-postorbital contact, represented a kinetic joint between the bones of the skull roof (intertemporal and supratemporal) and the cheek (postorbital and squamosal), both in *C. scoticus* and other early tetrapods (Panchen, 1975). CT scans demonstrate that the squamosal-supratemporal contact was undulating, making mobility at this joint unlikely (for further examination of potential kinesis in the skull of *C. scoticus*, please see Discussion). The anteromedial margin of the supratemporal makes a short, interdigitated contact with the parietal. Posteriorly, the medial edge of the supratemporal meets the lateral margin of the postparietal in a strongly interdigitated contact. The posterior margin of the supratemporal contacts the anterior margin of the tabular in strongly interdigitated suture. The posterolateral edge of the supratemporal is strongly anteriorly concave and smooth, forming the anteromedial margin of the otic notch.

Tabular—The tabular, which is preserved on both sides of NHMUK VP R10000, is a robust, triangular bone with its apex directed posteriorly (Figs. 2C, D). In transverse section, the tabular is rounded laterally and tapers medially. Scans reveal a large amount of porous bone within the anterior part of the tabular. The medial margin of the tabular is dorsally overlapped by the lateral margin of the postparietal in a strongly interdigitated suture. The medial half of the dorsal surface is sculpted, resembling other bones of the skull roof; the lateral margin is smooth and rounded, forming the medial margin of the otic notch. The tabular horn is round in cross section and smooth, tapering to a rounded point. The posterodorsal margin of the tabular is sharp; ventral to this shelf, the posterior aspect of the tabular is smooth and strongly embayed, forming a pronounced concavity that contributed to the occiput. The lateral half of the ventral aspect of the tabular is smooth and convex; medially, the ventral aspect of the tabular is marked by two large, rugose facets surrounded by raised lips, which extend onto the postparietal (Fig. 2D). Panchen (1985) suggested these facets marked the contact between the tabular and the opisthotic, which is not preserved.

Postparietal—The postparietal is a square-shaped bone in dorsal view and forms part of the posterior margin of the cranium and occiput (Fig. 2C, D, S6A, B). It is preserved on both sides of NHMUK VP R10000, although the left element has been badly broken. In transverse section, the postparietal is depressed medially and dorsally arched laterally. The postparietals appear to meet at a midline butt joint, however, the specimen has been broken through this contact. Laterally, the posterior surface of the postparietal is embayed and bears a concavity that continues onto the posterior aspect of the tabular; medially, the postparietal bears a distinct rounded projection from its posterior surface. As described by Panchen (1985), the dorsal surface of this tabular is concave and the ventral surface convex. The posterolateral margin of the ventral aspect of the postparietal is marked by a pair of rugose facets that extend onto the tabular (Fig. 2D) and presumably contacted the opisthotic (Panchen, 1985).

Palate

Vomer—Both vomers are preserved in NHMUK VP R10000 and NHMUK PV OR30532, with the left element of NHMUK PV OR30532 being the least disrupted (Figs. 2B, H, 4C, S7A–D). The vomer is composed of the mediolaterally and dorsoventrally expanded main body, which bears enlarged fangs. A process projects medially and anteriorly from the main body to meet its counterpart at the midline; a second process projects posteriorly from the main body to meet the pterygoids and palatines. Both processes bear teeth. In transverse section, the anterior part of the vomer features the dorsoventrally expanded main body and tapering anteromedial process; the posterior part of the vomer is 'L'-shaped in transverse section with a ventrally projecting lamina (posterior process) located laterally and a tapering medial lamina that dorsally overlaps the pterygoid. The vomerine fang is slightly posteriorly recurved in lateral view and slightly medially directed in anterior view. The fang base is circular in cross section and tapers to a fine point distally. Both sides of NHMUK VP R10000 and the right side of NHMUK PV OR30532 preserve a single fang whereas the left vomer of NHMUK PV OR30532 preserves two fangs. Both anteromedial processes of NHMUK VP R10000 and the right side of NHMUK PV OR30532 bear two small, posteriorly recurved teeth; the anteromedial process on the left side of NHMUK PV OR30532 bears two teeth and one empty socket. On both sides of NHMUK VP R10000, only one small, medially recurved tooth remains in the posterior process; however, nearby loose teeth and poorly preserved sockets suggest more teeth were originally present in the posterior process. The posterior processes of NHMUK PV OR30532 preserve three teeth on the left and one on the right.

The anterior margin of the vomer, composed of the main body and anteromedial process, is strongly embayed to form the posterior wall of the anterior palatal fossa, which is dorsally confluent with the interpremaxillary fenestra and presumably accommodated the adsymphysial teeth with the jaws closed. The anteromedial processes meet at an interdigitated midline contact and extend anteriorly to form the medial margins of the anterior palatal fossa. Posterior to the enlarged fang, the lateral margin of the vomer is strongly embayed to form the anterior and medial walls of the internal choana. The posterior process of the vomer tapers to a fine tip that ventrally underlaps the anteromedial margin of the palatine, with coarse interdigitations visible in this contact.

Palatine—The palatine is roughly teardrop-shaped, being mediolaterally and dorsoventrally expanded anteriorly and tapering posteriorly, and bears a medial process at its anterior end (Figs. 2B, H, 4C, S7E–G). The left palatine of NHMUK VP R10000 lacks its medial margin while the posterior portion of the right palatine is broken. Both palatines are present in NHMUK PV OR30532, with the left element being better preserved. Anteriorly, the palatine is dorsoventrally expanded at the level of the enlarged fang and tapers medially in transverse section; posteriorly, the palatine is triangular in cross section with the apex (bearing the teeth) ventrally directed (Fig. 7F). Both sides of NHMUK VP R10000 and NHMUK PV OR30532 bear a large fang roughly at the anteroposterior midpoint of the palatine; additionally, both sides of NHMUK PV OR30532 and the right side of NHMUK VP R10000 feature a resorption pit medial to the fang. The enlarged palatal fang is similar in shape to the vomerine fang. The portion of the palatine medial and anterior to the fang bears a series of small teeth that are vertical in anterior view and recurved in lateral view. The left palatine of NHMUK VP R10000 bears one tooth in this region while the right palatine bears three teeth; the left palatine of NHMUK PV OR30532 bears two teeth while no teeth are preserved on the right. Posterior to the fang there is a series of small, medially recurved teeth. The left palatine of NHMUK VP R10000 features six teeth in this region while the broken right palatine preserves two teeth; the right palatine of NHMUK PV OR30532 preserves four teeth posterior to the fang. The region posterior to the left palatal fang in NHMUK PV OR30532 is difficult to interpret. There is a second large fang followed by fragments of at least four teeth. Clack (1996)

identified this region as the palatine, in which case the left side of NHMUK PV OR30532 is unique in possessing two functional fangs and a resorption pit. Scans reveal a great deal of broken bone in this region; alternatively, this second fang and succeeding teeth may belong to the left ectopterygoid, which has been anteriorly displaced.

The anterior margin of the palatine is embayed to form the posterior margin of the internal choana. A short process extends from the anterolateral corner of the palatine and contacts the medial aspect of the maxilla in a laterally convex butt joint. At the level of the enlarged palatine fang, the maxilla-palatine contact becomes extensive and interdigitated, and the dorsolateral surface of the palatine contacts the ventromedial edge of the lacrimal in an interdigitated contact; additionally, as previously mentioned, a large medial projection of the lacrimal overlies the palatine dorsal to the fang. The medial margin of the palatine is ventrally underlapped by the lateral margin of the pterygoid and the posterior end of the palatine contacts the anterior end of the ectopterygoid. No interdigitations can be seen, and the palatine-ectopterygoid contact has been disrupted in all specimens.

Ectopterygoid—The ectopterygoid of *C. scoticus* is an anteroposteriorly elongate and mediolaterally narrow element, being transversely widest at its anterior end and tapering posteriorly (Figs. 2B, H, 4C, S7H–K). It is preserved on both sides of NHMUK VP R10000 and on the right side of NHMUK PV OR30532; as previously noted, it is unclear whether a tooth-bearing bone on the left side of NHMUK PV OR30532 represents the posterior portion of the palatine or the anteriorly displaced ectopterygoid. In transverse section, the ectopterygoid is expanded at the level of the enlarged fang and tapers medially and dorsolaterally to form shelves. The lateral shelf contacts the medial surface of the maxilla and ventral margin of the jugal (and, in NHMUK VP R10000, makes a point contact with the lacrimal). The medial shelf of the ectopterygoid is ventrally underlapped by the lateral margin of the pterygoid.

The dentition of the ectopterygoid varies between specimens and between sides. The left ectopterygoids of NHMUK VP R10000 and NHMUK PV OR30532 bear a single fang at their anterior ends; in contrast, the right ectopterygoid of NHMUK VP R10000 features two enlarged fangs plus a smaller tooth anterior to these fangs. The ectopterygoid fangs are approximately half the height of the vomerine and palatine fangs, and are nearly vertical in lateral view, being slightly medially curved. Posterior to the fangs, the ectopterygoid bears a row of small teeth that decrease in size posteriorly. The left ectopterygoid of NHMUK VP R10000 features 12 teeth and two empty sockets while the right element exhibits 13 teeth; the right ectopterygoid of NHMUK PV OR30532 exhibits 12 teeth. The posterior margin of the ectopterygoid forms the anterior margin of the subtemporal fossa.

Pterygoid—The pterygoid is the largest bone of the palate and is composed of anterior and quadrate processes, and the main body (=palatal ramus of Panchen [1985]). Both pterygoids in NHMUK VP R10000 are largely complete, with the left pterygoid being better preserved than the right. Both pterygoids of NHMUK PV OR30532 are badly fragmented, although their anterior processes are largely intact and clearly visible (Figs. 2B, H, 4C, S8).

The elongate anterior process of the pterygoid extends from the level of the medial process of the palatine to the level of the vomerine fang. These anterior pterygoid processes are the spongy bone discussed by Clack (1996) and later correctly identified by Clack (1998b). Posteriorly, the anterior process is a ventrally arched horizontal lamina that ventrally underlaps the medial shelves of the vomer and medial process of the palatine in an extensive contact; anteriorly, the bone increases slightly in dorsoventral height and underlaps the medial and posterior margins of the main body of the vomer. The anterior processes of the pterygoids meet at a tight and sinuous midline butt contact. Posterior to the medial process of the palatine, the pterygoid expands laterally to form the main body. In transverse section, the pterygoid is dorsoventrally tallest near (but not at) its medial margin; the medial half of the pterygoid is ventrally arched while the lateral half is dorsally arched (Fig. 7D). This cross-sectional morphology forms a subtle, broad longitudinal ridge along the ventral aspect of the main body of the bone. The lateral margin of the pterygoid underlaps the medial margins of the palatine and ectopterygoid. This is a smooth lap joint with no interdigitations, although a sliding joint between the marginal palatal bones and pterygoids, as suggested for some early tetrapods by Beaumont (1977) seems unlikely; see Discussion for more details.

Posterior to the level of the ectopterygoid fangs, the elongate cultriform process of the parasphenoid inserts between the pterygoids in NHMUK VP R10000. The anterior part of the parasphenoid is preserved and reaches the level of the medial process of the palatine in NHMUK PV OR30532 (Fig. S8D, E). Scans of NHMUK PV OR30532 demonstrate that the rounded medial margins of the pterygoids meet the lateral aspect of the parasphenoid in a rounded butt joint. There is no evidence from either specimen to suggest that the parasphenoid reached the vomers, contra reconstructions by Panchen (1985) and Clack (1996), but resembling Clack (1998b). The medial margin of the pterygoid becomes progressively thicker and rounded in cross section approaching the basal articulation (Fig. 7C), forming the concave socket that articulated with the ventral portion of the basipterygoid processes. This socket is circular, faces posteriorly and slightly medially, and is surrounded by a raised lip of bone. At the level of the basal articulation, the pterygoid and ectopterygoid separate and the main body of the pterygoid abruptly narrows mediolaterally, its free lateral edge forming the medial margin of the subtemporal fossa. In ventral view, the posterior part of the main body is sickle-shaped, initially curving medially, then turning laterally and terminating at a fine point (Fig. S8B). The ventral surface of the main body is covered with a fine shagreen of denticles (Clack, 1996; Panchen, 1985); in contrast, the dorsal surface is smooth.

The quadrate ramus of the pterygoid (Fig. S8A–C) consists of a dorsolaterally directed sheet of bone that rises from the medial margin of the main body immediately posterior to the basal articulation. The quadrate ramus increases in height posteriorly and the dorsal margin thickens and develops a deep groove—as described by Panchen (1985)—which articulates with the dorsomedial margin of the squamosal; this contact is best preserved on the right side of NHMUK VP R10000. At its posterior limit, the ventrolateral face of the quadrate ramus extensively overlaps the dorsomedial aspect of the quadrate.

Braincase

Sphenethmoid—Panchen (1985) states that the ventral margin of the sphenethmoid is visible above the cultriform process of the parasphenoid in NHMUK VP R10000 and Clack (1996) reports a part of the sphenethmoid associated with the anterior end of the cultriform process in NHMUK PV OR30532. The location of the sphenethmoid is not figured for either specimen. Scans reveal two unidentified bone fragments near the anterior end of the cultriform process in NHMUK VP R10000, including the piece that Panchen (1985) incorrectly identified as the preopercular. It is possible that these represent remnants of sphenethmoid but this is uncertain and no useful anatomical data can be extracted.

Parabasisphenoid—Scans reveal no visible suture between the parasphenoid and basisphenoid; thus, the two bones are treated as a single element in this description. The parabasisphenoid is more complete in NHMUK VP R10000; only its anterior end

and the posterior portion of the right side is missing. Only the anterior half of the basisphenoid is preserved in NHMUK PV OR30532, although this specimen preserves the anterior part of the cultriform process (Figs. 2A, H, 4C, S9A–E).

The cultriform process is dorsoventrally tallest at its base and tapers anteriorly. It also narrows mediolaterally at its midsection; NHMUK PV OR30532 demonstrates the parasphenoid expands transversely slightly at its anterior end (Fig. S9E). The cultriform process inserts between the pterygoids and contacts their medial margins at rounded butt joints. Scans reveal that the dorsal surface of the parasphenoid features a deep groove near the base of the process (Fig. S9B); anteriorly, the element flattens and the groove disappears. It is possible that this groove supported a cartilaginous midline sphenethmoid. Scans also reveal porous bone within the parasphenoid. The patch of denticles on the ventral aspect of the anterior cultriform process (Clack, 1996) could not be discerned in CT scans due to the very small size of these features and available scan resolution. As previously discussed, the cultriform process reaches the level of the medial processes of the palatines and there is no evidence to suggest a vomer-parasphenoid contact.

The basisphenoid is triangular in ventral view with its apex directed anteriorly (Fig. S9A). The sharp ventral keel of the posterior parasphenoid, which bears fine anteroposterior striations (Panchen, 1985), divides into two strong ridges at the level of the basal articulation. These ridges diverge posterolaterally on the ventral aspect of the basisphenoid (Fig. S9A). Between these ridges is a deep, triangular midline concavity with its apex directed anteriorly; the anterior part of this concavity is preserved in NHMUK PV OR30532. Posteriorly, the concavity flattens and the depression disappears near the center of the basisphenoid; however, the bounding ridges continue posterolaterally and support rounded, dorsoventrally expanded flanges that ventrally and laterally clasped the basioccipital. The posterior margin of the basisphenoid is V-shaped in ventral view.

The basipterygoid processes project anterolaterally and slightly dorsally; they are dorsoventrally expanded (Fig. S9A–D). Each features a rounded ridge on its anterior aspect (articular surface) which courses ventrolaterally and divides the articular surface into a smaller, convex ventral facet (that contacted the articular facets of the pterygoid) and a larger, concave dorsal facet (that contacted the conical recess of the epipterygoid). The basipterygoid process has a sharp lateral margin and is supported posteriorly by a strong, rounded buttress that courses posterodorsally. The junctions between the ventral ridges and the sharp lateral margins of the basipterygoid processes are marked by a notch; thus, the basisphenoid is butterfly-shaped in anterior view (Fig. S9C). The ventrolateral aspect of the basisphenoid between this buttress and the ventral ridge is depressed into a basipterygoid recess marking the course of the internal carotid artery. Dorsally, there is a shallow circular depression between the basipterygoid processes (Fig. S9B). Posterior to the processes, the lateral walls of the basisphenoid expand dorsally and bound a wide, U-shaped depression that floored the braincase and underlapped the anterior end of the basioccipital.

Epipterygoid—This endochondral component of the palatoquadrate is preserved only on the right side of NHMUK VP R10000 (Figs. 2A, S9F–I). Unlike *Acanthostega*, in which the epipterygoid is indistinguishably fused to the pterygoid (Porro et al., 2015b), the element is distinct in *C. scoticus* and composed of an anterior palatal ramus, the thickened columella cranii with the conical recess at its base, and the mediolaterally thin quadrate ramus. The palatal ramus is a short, dorsoventrally flattened sheet of bone that dorsally overlapped the main body of the pterygoid anterior to the basal articulation. The epipterygoid thickens posteriorly to form a buttress that anteriorly supports the basal articulation, then arcs posterodorsally as the columella cranii, which forms a thickened 'leading edge' to the quadrate ramus of the pterygoid. The base of the columella cranii and buttress of the anterior palatal ramus form a conical recess (Fig. S9F, H, I), which originally articulated with the anterior and dorsal portions of the basipterygoid process; however, the parabasisphenoid is posteriorly displaced and the joint is open in NHMUK VP R10000. The recess is semicircular and faces posteroventrally and medially. The basal articulation appears to have been synovial in *C. scoticus* (Clack, 1992; Panchen, 1985) as in *Acanthostega* (Porro et al., 2015b). The columella cranii bears a mediolaterally thin flange of bone on its posterior margin. This forms the quadrate ramus that laterally overlaps the anterior margin of the quadrate ramus of the pterygoid.

Basioccipital—The complete basioccipital is preserved in NHMUK VP R10000 although the element is displaced far posterior to the skull and was scanned with the postcrania (Fig. 2E, F). In external view, there are distinct ventral and lateral surfaces. The ventral surface is widest posteriorly, narrows slightly anteriorly, and is separated by faint ridges from the lateral surfaces, which were clasped by the posterior arms of the basisphenoid. The lateral and ventral surfaces are anteroposteriorly arched and bear numerous minute pits as noted by Panchen (1985); CT scans reveal that these pits lead to a maze of porous bone (Fig. 7B) within the basioccipital. The ventral margin of the anterior end of the basioccipital is bilobed with a semicircular median notch. There are two deep concavities on the anterodorsal surface separated by a median ridge with a longitudinal midline groove. Panchen (1985) speculated these concavities and grooves housed extensions of the cartilaginous exoccipitals. The posterodorsal surface of the basioccipital bears two deep concavities bounded laterally by the dorsoventrally expanded lateral margins of basioccipital and separated by a rounded midline ridge. Panchen (1985) identified the concavities as junctions for the exoccipitals and the notochord. The sharp posteroventral margin of the basioccipital formed part of the occipital condyle and is semicircular in posterior view and nearly straight in ventral view.

Lower Jaw

This description of the lower jaw (Figs. 3, 5) is based on three of the scanned specimens: the complete lower jaws of NHMUK VP R10000, which measure 328 mm in total length; GSE 4722, which measures 320 mm in length; and NHMUK VP R310, which measures approximately 320 mm in length based on a restoration by Panchen (1985) prior to being broken (see also Clack et al., 2018). The lateral aspect of the *C. scoticus* lower jaw (Fig. 5A) is made up of the dentary and four infradentary bones. The medial face is made up of the prearticular, three coronoid bones and the adsymphysial, and the medial laminae of the splenial and angular (Fig. 5B). In lateral view the ventral margin of the lower jaw is curved, with the curvature becoming more pronounced posteriorly. The ventromedial apex of the splenial and ventral margins of the postsplenial, angular, and surangular form a distinct keel (Panchen, 1985) that courses from the anterior end of the splenial to a point posterior to the jaw joint. The dorsal margin of the lower jaw is straighter than the ventral margin, with several subtle undulations on the tooth-bearing dentary. There is no surangular or coronoid crest, and the lower jaw is dorsoventrally tallest midway between the posterior end of the tooth row and the jaw joint. The Meckelian fenestra is a ragged opening between the uneven ventral margins of the prearticular and the infradentary bones, stretching from the medial lamina of the splenial (anteriorly) to the medial lamina of the angular (posteriorly).

In dorsal view (Fig. 5C), the lateral and medial margins of the lower jaw are parallel along its entire length, with the front of the ramus curving medially to meet its counterpart at the symphysis.

The mandibular adductor fossa occupies the posterior third of the lower jaw. The specimens exhibit varying numbers of deep pits or fossae on the dorsal surface of the lower jaw, anterior to the mandibular adductor fossa; additionally, the bones forming the margins of these fossae differ between specimens (see Discussion). In all three specimens, the most anterior opening, located medial to the dentary tusk, represents a tooth replacement pit. The more posterior fossae accommodated the enlarged palatal fangs when the jaws were closed as demonstrated in the articulated jaws of NHMUK VP R10000. Despite the naming conventions used below, it is unclear whether these fossae are homologous or analogous with the pre- and intercoronoid fossae of earlier stem tetrapods (Jeffrey, 2003), see Discussion for more details. Intercoronoid fossae also occur in some temnospondyls, such as *Dendrerpeton* (Arbez et al., 2022), suggesting these may be more widely distributed characters. The second fossa is an anteroposteriorly elongate opening at the anterior end of the lower jaw that accommodated the vomerine fang. It is equivalent in position to the precoronoid fossa of earlier stem tetrapods. The third fossa, referred to here as the first intercoronoid fossa, occurs just anterior to the contact between anterior and middle coronoids, and accommodates the palatine fang. The fourth fossa, referred to here as the second intercoronoid fossa, accommodates the ectopterygoid fang. GSE 4722 features an additional fossa midway between precoronoid and first intercoronoid fossae; this fossa is located medial to several enlarged dentary teeth and probably represents a tooth replacement pit.

Dentary—In lateral view (Figs. 3A, D, E, F, 5A, S10A), the dentary is dorsoventrally tallest anteriorly with its dorsal and ventral margins parallel for most of its length; it tapers posterior to the end of the tooth row and terminates as a spike overlying the surangular. In dorsal view (Figs. 5C, S10B), the dentary tapers posteriorly and widens slightly anteriorly to form the symphysis. The anterior tip of the dentary accommodates an enlarged tooth (see below) and a replacement pit. At this level, the dentary is U-shaped in transverse section, with the lateral lamina supporting teeth, the ventral lamina flooring the precoronoid fossa, and the medial lamina contacting the splenial and adsymphysial. Posteriorly, the dentary is laterally bowed in cross section with a thickened dorsal margin bearing the teeth, a mediolaterally thin ventral margin that contacts the infradentary bones, and a robust medial shelf that contacts the coronoid series; this shelf is most extensive anteriorly and becomes less pronounced posteriorly.

As noted by previous authors, the lower jaw dentition of *C. scoticus* is strikingly heterodont compared with that of the upper jaw (Ahlberg & Clack, 1998; Panchen, 1985) with alternating groups of large and small teeth, resembling the condition in crocodilians, although the latter exhibit heterodonty (in tooth size) in both the upper and lower jaws. The early tetrapods *Acherontiscus* (Clack et al., 2019) and *Greererpeton* (Bolt & Lombard, 2001), some baphetids such as *Megalocephalus* (Beaumont, 1977), and the temnospondyl *Balanerpeton* (Milner & Sequeira, 1994) also feature lower teeth that are larger than those of the upper jaw and exhibit heterodonty in tooth size. Also, as in crocodilians, the upper margin of the dentary has subtle undulations that correspond to changes in tooth size, with larger teeth located on peaks; these undulations are most visible in NHMUK VP R10000. All specimens exhibit an enlarged anterior dentary tusk, and unlike earlier stem tetrapods (see discussion in Porro et al., 2015a) these tusks are in line with (rather than medial to) the marginal dentition. Posteriorly, there are two subsequent regions of enlarged teeth, between the pre- and intercoronoid fossae. Thus, the enlarged dentary teeth alternated in anteroposterior position with the large palatal fangs in the articulated skull. Enlarged teeth in line with the marginal dentition are a diagnostic feature of colosteids, such as *Greererpeton*, *Colosteus*, and *Deltaherpeton* (Bolt & Lombard, 2010; Hook, 1983; Smithson, 1982), although other groups of early tetrapods also express this character. The teeth are gently recurved in lateral view; in anterior view, they have a pronounced medial curvature.

The left dentary of NHNUK VP R10000 features 38 teeth, including one small tooth; one tusk followed by four smaller teeth and two empty alveoli; three enlarged teeth; seven small teeth; one enlarged tooth and 15 small teeth plus five alveoli. The damaged right dentary of NHMUK VP R10000 features 27 teeth, including one small tooth; one tusk followed by six smaller teeth; one enlarged tooth; five small teeth and one alveolus; two enlarged teeth; and seven small teeth with three alveoli. GSE 4722, which is badly broken across its center, features 31 teeth, including one small tooth; one tusk followed by five smaller teeth and three alveoli; three enlarged teeth; two small teeth; one enlarged tooth; 10 small teeth and five alveoli. NHMUK VP R310 features 38 teeth, including two small teeth; one tusk followed by six smaller teeth and two alveoli; one enlarged tooth; six small teeth; three enlarged teeth; and 17 small teeth. Although the scanned specimens sustained varying amounts of damage, it would appear the dentary tooth count in *C. scoticus* was somewhat lower than Panchen's (1985) estimate of 45 teeth, and substantially lower than the total premaxillary/maxillary tooth count.

Only NHMUK VP R10000 preserves both lower jaws, which are disarticulated at the symphysis. Nonetheless, examination of specimens and CT scans gives insight into the nature of the mandibular symphysis in *C. scoticus*. Unlike earlier stem tetrapods, the Meckelian canal of *C. scoticus* terminates posterior to the dentary tusks and does not open onto the symphysis (Porro et al., 2015a, 2015b). Except for the articular, there is no evidence for ossified Meckelian bone within the lower jaw of *C. scoticus* and presumably this canal was filled with Meckel's cartilage in life (Ahlberg & Clack, 1998). The dentaries contacted each other at a flat, porous surface that is nearly circular in medial view and posteriorly bounded by anterior extensions of the adsymphysial and splenial; the morphology and surface texture suggest a loose butt contact (Fig. S10C). Anterior to the symphysis there is a rugose area interpreted as the attachment site of symphysial ligament (Panchen, 1985). At the level of the tusk, the dorsomedial margin of the dentary is capped by the adsymphysial in an interdigitated contact. The anterior coronoid wedges between the dentary and adsymphysial in NHMUK VP R10000 and NHMUK VP R310; posteriorly, the medial shelf of the dentary broadly overlaps the dorsolateral aspect of all three coronoids in a strongly interdigitated contact. Anteriorly, the splenial underlaps the dentary in an interdigitated contact; posterior to the tusk, the dorsolateral margin of the splenial fits into a groove in the ventral margin of the dentary. The ventral margin of the dentary laterally overlaps the dorsal margins of the postsplenial, angular, and surangular in extensive scarf joints, posteriorly tapering to a point that overlies the surangular; this pattern of contact between the dentary and infradentary series appears to be highly conserved among stem tetrapods (Porro et al., 2015a, 2015b). The medial shelf of the dentary appears to overlie the dorsal margin of the prearticular in NHMUK VP R310 but this is almost certainly due to deformation; in NHMUK VP R10000, there is no contact between the dentary and prearticular.

The external surface of the anterior dentary is covered in irregular pores and pits; scans reveal that the anterior dentary of *C. scoticus* is highly porous, presumably for vasculature or nerves. Posteriorly, the external surface of the dentary is marked by a series of fine, anteroposteriorly oriented striations.

Splenial—The splenial (Figs. 3, 5B, D, S10E–G) is an elongate bone forming the anteroventral margin of the lower jaw. As in other stem tetrapods (Porro et al., 2015a, 2015b), the splenial is

V-shaped in transverse section (Fig. 7G). The apex is ventromedially directed, forming the sharp ventral keel of the anterior lower jaw. One arm of the V forms the lateral lamina, which contacts the dentary and postsplenial. The second arm forms the medial lamina, which contacts the adsymphysial, anterior coronoid, and prearticular. The lateral lamina is laterally bowed in cross section, whereas the medial lamina is depressed (although this is less pronounced than in either *Eusthenopteron* or *Acanthostega*, as figured in Porro et al. [2015a, 2015b]).

The anterior end of the splenial posteroventrally bounds the symphysial region of the dentary, and it seems likely that the splenials contacted each other at a short, semicircular midline butt joint continuous with the dentary-dentary contact surface (Fig. S10F). The lateral lamina of the splenial overlaps the anterior margin of the postsplenial; compared with other early tetrapods, however, this contact is anteroposteriorly short and may represent a potential weak point in the lower jaw, especially given that all specimens have experienced breakage in this region. Anteriorly, the medial lamina ventrally and medially overlaps the adsymphysial in an interdigitated contact. This is continuous with the overlapping, interdigitated contact between the medial lamina of the splenial and anterior coronoid. In NHMUK VP R10000 and NHMUK VP R310, the medial lamina bifurcates posteriorly into a short dorsal process (=mesial lamina of Clack et al., 2018) and a longer ventral process. The short dorsal process medially overlaps the anterior process of the prearticular, which wedges between the splenial and anterior coronoid. The ventral process forms part of the ventral margin of the Meckelian fenestra.

The lateral line of the lower jaw forms a conspicuous open groove on the lateral face of the lower jaw, immediately dorsal and parallel to the ventral border of the lower jaw (Fig. S10G). It begins near the anterior end of the splenial and continues to the posterior end of the surangular. Ornamentation above and below the groove on the splenial consists of anteroposteriorly elongated grooves and ridges. CT scans demonstrate that small openings within the groove lead into a porous area within the bone, best seen in scans of NHMUK VP R310; however, no single canal can be discerned. A canal running through the lower jaw was preserved in UMZC 2011.9.1 (Clack et al., 2018); however, scans demonstrated this canal did not connect to the lateral line.

Postsplenial—The postsplenial is similar in length to the splenial (Figs. 3, 5A, D, S11A). The anterior margin is blunt in NHMUK VP R10000 and NHMUK VP R310 but tapering in GSE 4722; in all specimens, the postsplenial tapers posteriorly. In transverse section, it is laterally bowed with a thickened ventral margin and tapering dorsal margin. The dorsal margin of the postsplenial broadly overlaps the lateral aspects of the anterior and middle coronoids in GSE 4722; however, this is almost certainly due to deformation of this specimen. It is possible that the dorsal margin of the postsplenial and lateral aspect of the middle coronoid met in a short butt contact as in NHMUK VP R10000 and NHMUK VP R310. In all specimens, the postsplenial laterally and ventrally laps the angular in an extensive and strongly interdigitated contact that is nearly horizontal in lateral view, terminating as a rounded point underlying the angular. The ventromedial margin of the postsplenial forms part of the ventral margin of the Meckelian fenestra and makes point contacts with the ventral margin of the prearticular; however, these are almost certainly due to deformation, as discussed in Clack et al. (2018). The groove marking the lateral line system continues from the splenial onto the ventrolateral aspect of the postsplenial. As with the splenial, some short canals lead from this groove into the bone but there is no internal canal. Ventral to the groove, the external surface of the postsplenial is marked by elongate ridges and grooves; dorsally, it is covered in shorter grooves and pits.

Angular—The angular is preserved on both sides of NHMUK VP R10000 and is mostly complete in GSE 4722; only the anterior half is preserved in NHMUK VP R310 (Figs. 3, S11B–E). It is tallest at its midsection, tapering anteriorly and posteriorly. As with the postsplenial, it is laterally bowed in transverse section with a tapering dorsal margin. Anteriorly, the thickened ventral margin of the angular forms the margin of the Meckelian fenestra. The posterior halves of the angulars in NHMUK VP R10000 and GSE 4722 preserve a mesial lamina (Figs. 3C, E, F, S10C, E), a mediolaterally thick and dorsoventrally short flange of bone that rises from the ventral margin of the angular and forms part of the medial aspect of the lower jaw (Clack et al., 2018); the mesial lamina is missing in NHMUK VP R310. The thickened ventral margin of the prearticular passes internal (lateral) to the mesial lamina of the angular and the two bones make several weak point contacts (Clack et al., 2018). The ventral margin of the surangular extensively overlaps the dorsal margin of the angular in a smooth scarf without interdigitations. The dorsal margin of the angular makes short point contacts with the middle and posterior coronoids in NHMUK VP R10000 and NHMUK VP R310, although these may be due to deformation.

The groove of the lateral line continues along the ventrolateral aspect of the angular (Fig. S11B, D). CT scans of NHMUK VP R10000 (both sides) and GSE 4722 reveal a longitudinal canal that arises at the anteroposterior midpoint of the angular and continues posteriorly; this large internal canal connects via small canals to the external groove. In GSE 4722 and on the right side of NHMUK VP R10000 the canal opens onto the lingual aspect of the angular ventral to the mesial lamina. It is unclear whether this is the same structure visualized along the entire lower jaw of UMZC 2011.9.1 (Clack et al., 2018). The external ornamentation of the angular consists of longitudinal grooves ventral to the lateral line; dorsal to the lateral line, shallow grooves radiate outwards and dorsally from the anteroposterior center of the angular.

Surangular—The surangular forms the posterolateral part of the lower jaw and is preserved (although damaged) on both sides of NHMUK VP R10000; its anterior portion is preserved in both NHMUK VP R310 and GSE 4722 (Figs. 3, S11F, G). It is elliptical in lateral view (Fig. 5A), tapering anteriorly and posteriorly, with a nearly straight dorsal margin and a curved posteroventral margin. In dorsal view, the surangular forms most of the lateral margin of the mandibular adductor fossa (Fig. 5C). It is gently laterally bowed in transverse section, with a tapering ventral margin and a thickened dorsal margin; this thickening is more pronounced posteriorly. The anterior process of the surangular inserts between the dentary and angular. In NHMUK VP R10000 and NHMUK VP R310, the dorsal margin of the surangular meets the lateral aspect of the posterior coronoid in an interdigitated suture. The posterior part of the surangular wraps around and overlaps the lateral and posterior aspects of the articular. No interdigitations occur at this suture, although larger-scale ridging is visible in scans (Clack et al., 2018). The posterior margin of surangular does not contact the posterior margin of the prearticular. Near its posterior end, the dorsal margin of the surangular is drawn up into a sharp crest, delineating the anterior margin of the jaw joint. Behind this, the dorsal surface of the element is deeply depressed, forming the lateral part of the jaw joint as noted by Panchen (1985). The posterior tip of the surangular is pointed and strongly dorsally curved, and posteriorly bounded and constrained the jaw joint; it also marks the posterior end of the ventral keel.

The lateral line groove continues parallel to the posteroventral margin of the surangular (Fig. S11F) and terminates below the jaw joint. The lateral surface of the anterior process of the surangular is covered in fine longitudinal striations. Posteriorly and

dorsal to the lateral line, the surangular features elongated grooves and pits radiating from a point ventral to the jaw joint.

Adsymphysial—The adsymphysial (also known as the parasymphysial plate) of *C. scoticus* was first described by Ahlberg and Clack (1998) (Figs. 3B, C, E, F, S12A, B). It is elongate and both mediolaterally widest and dorsoventrally tallest at its rounded anterior margin, tapering posteriorly to a point. In GSE 4722, it forms the medial wall of the precoronoid fossa. Anteriorly, the adsymphysial curves dorsally and is square in transverse section, contacting the dentary laterally and the splenial ventromedially. The concave medial surface of the anterior adsymphysial is continuous with the symphysial surface of the dentary, indicating where the adsymphysial may have been joined to its counterpart across the midline by a strong ligament (Fig. S12B). The middle part of the right adsymphysial of NHMUK VP R10000 bears two teeth and a replacement pit whereas the right side preserves a single tooth. The adsymphysial dentition is best preserved in NHMUK VP R310, which features three teeth that are strongly posteriorly recurved (Figs. 3A, S12B). The toothrow is bordered medially by a deep concavity on the dorsal surface of the bone. The contact between the adsymphysial and anterior coronoid varies between specimens: the adsymphysial dorsally overlaps the anterior coronoid in NHMUK VP R310 and on the right side of NHMUK VP R10000, passes ventral to the anterior coronoid of GSE 4722, and there is no contact between the elements on the left side of NHMUK VP R10000. There is no contact between the adsymphysial and prearticular in any specimen.

Anterior Coronoid—The three coronoids are anteroposteriorly long and mediolaterally narrow bones (Figs. 3, 5, S12C–H), with the three bones being similar in length in NHMUK VP R310 but the posterior coronoid being substantially longer than the other two elements in NHMUK VP R10000. The anterior coronoid (Fig. S12C, D) is triangular in cross section, with the apex ventrally directed and a subtle lateral shelf that articulates with the dentary. The ventromedial surface contacts the medial lamina of the splenial and the prearticular, which wedges between the splenial and anterior coronoid, and extensively medially laps the latter bone. The tapering posterior process of the anterior coronoid inserts between the middle coronoid and dentary, with faint interdigitations visible at the contact between the coronoids in NHMUK VP R10000. The anterior coronoid forms the medial wall of the first intercoronoid fossa in NHMUK VP R10000. Panchen (1985) described teeth only on the first two coronoids whereas Ahlberg and Clack (1998) reported that there were no teeth on the anterior and middle coronoids. CT scans reveal that all three coronoids bear teeth, with three teeth in the right anterior coronoid and four in the left anterior coronoid of NHMUK VP R10000. The teeth are small, and both posteriorly and medially recurved.

Middle Coronoid—The middle coronoid is similar in length to the anterior coronoid in NHMUK VP R310 and GSE 4722; however, it is substantially shorter anteroposteriorly than the other coronoids in NHMUK VP R10000 (Fig. S12E, F). Its cross-sectional geometry is identical to that of the anterior coronoid and its ventromedial aspect is extensively lapped by the thickened dorsal margin of the prearticular, with interdigitations visible. The posterior tip of the medial coronoid inserts between the posterior coronoid and the dentary, with interdigitations visible between the coronoids. The middle coronoid forms the anteromedial margin of the second intercoronoid fossa in NHMUK VP R10000. Scans reveal the presence of five teeth and two empty sockets in the left middle coronoid of NHMUK VP R10000; the teeth are small and slightly medially recurved.

Posterior Coronoid—The posterior coronoid is similar in size to the other two coronoids in NHMUK VP R310 but nearly twice as long as the anterior coronoid in NHMUK VP R10000 (Fig. S12G, H). Its cross-sectional geometry resembles that of the other coronoids and its ventromedial aspect is extensively overlapped by the prearticular in an interdigitated contact. The posterior coronoid forms the posteromedial wall of the second intercoronoid fossa in NHMUK VP R10000 and contributes to the anterior margin of mandibular adductor fossa. The left posterior coronoid of NHMUK VP R10000 preserves 13 teeth and the right posterior coronoid exhibits 26 teeth and one empty socket; the teeth are very small and conical.

Prearticular—The prearticular forms most of the medial aspect of the lower jaw (Figs. 3, 5B, C, S13A–D) and was extensively described in Clack et al. (2018). It is preserved but damaged in both NHMUK VP R10000 and NHMUK VP R310. A mediolaterally thin sheet of bone with a thickened dorsal margin that has been dorsally displaced from the rest of the lower jaw in GSE 4722 may represent a portion of the prearticular. The prearticular is tallest at the mandibular adductor fossa, tapering anteriorly and posteriorly. The dorsal margin is nearly straight in medial view while the ventral margin follows the curve of the lower jaw, forming the ragged dorsal margin of the Meckelian fenestra. In transverse section, the prearticular is mediolaterally thin with a thickened dorsal margin (that contacts the coronoids) and a sharp ventral margin, and is either vertical or laterally bowed, although this may be due to deformation. Posteriorly, the ventral margin of the prearticular thickens where it passes internal to the mesial lamina of the angular; anteriorly, the prearticular tapers to a fine point that inserts between the splenial and anterior coronoid but does not reach the adsymphysial. The posterior part of the prearticular forms the entire medial margin of the mandibular adductor fossa before twisting strongly about its longitudinal axis and being broadly applied to the ventral and medial surfaces of the articular in a faintly interdigitated contact. Panchen (1985) and Ahlberg and Clack (1998) described the dorsal portion of the medial aspect of the prearticular, as well as the three coronoids, being covered in a shagreen field, but this cannot be visualized in CT scans.

Articular—The articular of *C. scoticus* is extensively lapped by the prearticular (medially) and surangular (laterally) so that only the jaw joint surface and a sliver of its posteromedial aspect are externally exposed (Figs. 3, 5, S13E–L). The articular is triangular in anterior view, with the base forming the nearly vertical lateral wall that meets the surangular and the apex medially directed. The ventromedial aspect contacts the prearticular and the dorsal aspect forms the jaw joint surface. The articular is also triangular in lateral view, with the apex forming the posterior tip of the lower jaw and the base forming the anterior aspect. The anterior aspect of the articular is deeply concave, both dorsoventrally and mediolaterally, forming the posterior wall of the mandibular adductor fossa (Fig. S13E, I). The ventromedial aspect, which is overlapped by the prearticular, is anteroposteriorly and dorsoventrally concave. In contrast, the lateral aspect, which is overlapped by the surangular, is convex (Fig. S13G, K). The ventral margin is sharp. The dorsal aspect (Fig. S13F, J), which forms the anteroposteriorly short and mediolaterally wide jaw joint, has a complex morphology: it is anteroposteriorly concave and mediolaterally convex, or "saddle-shaped," as described by Panchen (1985). The joint surface is posteriorly convex (U-shaped) and is bordered anteriorly and posteriorly by strong ridges that restricted anterior or posterior displacement of the quadrate relative to the articular. Finally, the joint surface is twisted about its transverse axis. Panchen (1985) described the joint surface as screw-shaped, with the medial part of the surface facing dorsally and the lateral part facing anteriorly; 3D reconstruction suggests that, in fact, the medial part of the joint surface was posterodorsally directed and the lateral portion dorsally directed.

Three-Dimensional Reconstruction

Numerous reconstructions of the skull of *C. scoticus* have been attempted. The earliest attempt was by Watson (1929), in which the holotype was mirrored and the bones of the skull roof were inferred from other tetrapods, resulting in an extremely broad skull and snout with a wide area between the orbits. The skull roof preserved in NHMUK VP R10000 permitted a very different reconstruction by Panchen (1985) in which he depicted *C. scoticus* with a dorsoventrally tall skull, a mediolaterally narrow and pointed snout, a very narrow interorbital region, small vomers, and narrow pterygoids separated by a wide interpterygoid vacuity. This reconstruction was the first to recognize the unusual interpremaxillary fenestra; it also featured a small naris and single midline anterior palatal fossa. Clack's (1996) examination of NHMUK PV OR30532 revealed the massive vomers and resulted in a new palatal reconstruction featuring a broader palate and more rounded snout, as well as wider pterygoids anteriorly separated by a massive parasphenoid. Further preparation of NHMUK PV OR30532 led to a revised reconstruction (Clack 1998b) in which the anterior processes of the pterygoids meet each other at the midline and underlap the vomers; posteriorly, the pterygoids contact the slender, median parasphenoid. In dorsal and lateral views, Clack's (1998b) reconstruction featured a shorter, broader snout and larger external naris than Panchen's (1985) and paired anterior palatal fossae. The lateral aspect of the lower jaw was most recently reconstructed by Panchen (1985), with a reconstruction of the medial surface presented by Ahlberg and Clack (1998).

The new 3D digital reconstruction is dorsoventrally shorter in lateral view than previous reconstructions (Fig. 4A). The three sets of palatal fangs project well below the ventral border of the skull. This flatter profile is due to the wide palate (Fig. 4C) and narrow interorbital region of the skull roof (Fig. 4B); as a result, the sides of the skull—traditionally depicted as nearly vertical (Clack, 1998b; Panchen, 1985) due to their preservation in the holotype—must be inclined at approximately 45° in order to articulate with both the palate and skull roof. In dorsal view (Fig. 4B), the snout is intermediate in shape between Panchen's (1985) and Clack's (1998b) reconstructions, featuring the distinct "pinching-in" at the premaxilla-maxilla junction noted by Clack (1998b). The sides of the skull diverge gently posteriorly, with the skull being widest across the midpoint of the quadratojugals; the sides then converge slightly towards the jaw joints. The new reconstruction features a L:W ratio of 1.7, which is wider than Clack's (1998b) reconstruction (1.9), and suggests that while the skull of *C. scoticus* was relatively narrower than those of most basally branching tetrapods (Bolt & Lombard, 2018), it was wider than the reconstructed skulls of *Proterogyrinus* and *Whatcheeria* (Bolt & Lombard, 2018; Rawson et al., 2021). The new reconstruction features a H:L ratio (ignoring the height of the very long palatal teeth) of 0.26. This resembles the H:L ratios of the skulls of most early tetrapods (Bolt & Lombard, 2018) and contrasts with previous reconstructions of *C. scoticus* as well as *Whatcheeria*, which both featured H:L ratios of 0.37 (Bolt & Lombard, 2018; Clack, 1998b; Rawson et al., 2021), suggesting a substantially flatter skull in *C. scoticus* than previously reported. Posterior to the orbit, the skull roof descends slightly posteriorly (Fig. 4A); this organization of the postorbital cranial vault is also seen in 3D and 2D reconstructions of the skulls of *Acanthostega*, *Ventastega*, *Parmastega*, and *Lethiscus*, and appears to have been widespread among early tetrapods (Ahlberg et al., 2008; Beznosov et al., 2019; Pardo et al., 2017; Porro et al., 2015b).

The 3D reconstruction exhibits orbits that are nearly 20% of total skull length, pentagonal in dorsal view, with a prominently pointed anteroventral corner. The preorbital region (tip of snout to anterior margin of orbit) is about 30% of total skull length while the elongated postorbital region is just over half (51%) of total skull length; this is a greater proportion of the skull than in other early tetrapods, including *Whatcheeria* (33%) (Rawson et al., 2021) and *Acanthostega* (47%) (Porro et al., 2015b). The dorsal aspect of the 3D model also features the enormous, tear-drop shaped interpremaxillary fenestra, an enlarged naris as reconstructed by Clack (1998b), and a slit-like otic notch.

Panchen (1985) illustrated the anterior palatal fossa as a single midline opening; in contrast, Clack (1996, 1998b) depicted a pair of openings separated by the anterior processes of the vomers contacting the posteriorly directed palatal processes of the premaxilla. In ventral view (Fig. 4C), the new reconstruction supports Clack's (1998b) interpretation of paired anterior palatal fossae and a midline contact between the anterior portions of the pterygoids. In contrast to earlier reconstructions, the 3D model suggests that the maxilla may have contributed to the posterolateral margin of the choana. This discrepancy is due to the preserved contacts between these bones in NHMUK VP R10000, the specimen primarily used for our 3D reconstruction, whereas earlier attempts reconstructed this region based on NHMUK PV OR30532, in which the maxilla is excluded from the choana. The 3D reconstruction exhibits enormous subtemporal fossae; the width of each opening is 38% of total maximum skull width. As described in the Methods, reconstructing the skull necessitated gentle dorsal vaulting of the palate. Although early tetrapods have traditionally been reconstructed with horizontal palates, the presence of a dorsally vaulted palate in *C. scoticus*, *Ichthyostega* (Rosen et al., 1981), *Acanthostega* (Porro et al., 2015b), and *Whatcheeria* (Bolt & Lombard, 2018; Rawson et al., 2021) suggests this assumption needs to be reevaluated. Lastly, the reconstruction reveals that the jaw joint (condylar surface of the quadrate) was not transversely oriented but anteromedially inclined in ventral view. Along with features previously described by Panchen (1985), this has implications for jaw movements (see Discussion).

Compared with earlier reconstructions by Panchen (1985) and Ahlberg and Clack (1998b), the lower jaw is less curved in lateral and medial views (Fig. 5A, B). Previous reconstructions of the lower jaw were based on NHMUK VP R310 and GSE 4722, both of which experienced strong mediolateral crushing, exaggerating the height of the lower jaw. The new reconstruction, based primarily on NHMUK VP R10000, suggests that the dorsal margin of the lower jaw was nearly straight, with no surangular eminence, and the ventral margin was gently curved. Otherwise, the arrangement of bones on both the lateral and medial aspects closely resembles previous reconstructions, and the articular is exposed posteriorly between the surangular and prearticular. In dorsal view (Fig. 5C), the lower jaws curve gently outwards from the symphysis, reaching their maximum mediolateral width at the posterior end of the dentary, then gently converge towards the jaw joints. The mandibular adductor fossa is rectangular in dorsal view and the jaw joint formed by the articular and surangular matches the condylar surface of quadrate in being anteromedially inclined.

DISCUSSION

New Anatomical Information and Intraspecific Variability

Computed tomography scanning and data processing have revealed new anatomical details of the cranium and lower jaws of *C. scoticus*, particularly by exposing the previously unseen palatal surface and dorsal margins of the lower jaws in NHMUK VP R10000, the lateral aspect of GSE 4722, and the medial aspect of NHMUK VP R310. Additionally, the internal surfaces of the bones in all specimens, as well as elements hidden between other bones due to taphonomic deformation, were visualized for the first time, including large parts of the

left jugal, squamosal, and the postorbital in NHMUK VP R10000. Our study supports the absence of a preopercular in *C. scoticus*, as well as the fact that the anterior tectal identified by Panchen (1985) actually represents the nasal; both points were previously suggested by Clack (1998b). We observed a greater number of maxillary teeth than previously reported, extending nearly the entire length of the maxilla. Scans support the arrangement of the anterior bones of the palate as reconstructed by Clack (1998b). Segmentation of CT data conclusively demonstrates the presence of teeth on the elongated adsymphysial and on all three coronoid bones. We also visualized the anterior process of the prearticular passing internal to the medial lamina of the splenial and lack of strong contacts between the prearticular and the postsplenial and angular (anterior to the mesial lamina) (Clack et al., 2018).

Our study revealed intraspecific variability between specimens and asymmetry within specimens, particularly in how some of the bones contact each other. For example, the lacrimal laterally overlaps the posterodorsal margin of the premaxilla in an interdigitating contact, excluding the maxilla from the external naris, in the holotype and on the left side of NHMUK PV OR30532. These bones make a point contact on the right side of NHMUK PV OR30532 and approach but do not contact each other in NHMUK VP R10000. The maxilla is excluded from the external naris by the lacrimal on both sides of NHMUK PV OR30532 but appears to contribute to the ventral narial margin on the left side of NHMUK VP R10000. In NHMUK PV OR30532, the rounded anteromedial margin of the maxilla extensively contacts the posterolateral aspect of the vomer in an interdigitated suture, excluding the premaxilla from the choana (Clack, 1996, 1998b); the maxilla-vomer contact is more limited on both sides of NHMUK VP R10000. The lacrimal contributes to the anteroventral corner of the orbit in NHMUK PV OR30532, but is excluded from the orbital margin by a point contact between prefrontal and jugal in the type (Clack, 1998b; Panchen 1973, 1985); disarticulation in this area prevents interpretation in NHMUK VP R10000. The direction of overlap between the lacrimal-jugal and jugal-quadratojugal scarf joints varies between the three cranial specimens, as does the extent to which the lacrimal and jugal contact the dorsal surfaces of the marginal palatal bones. CT scans show that the jugal externally laps the lacrimal on both sides of NHMUK VP R10000; conversely, the lacrimal externally laps the jugal on both sides of NHMUK PV OR30532. The posteroventral margin of the jugal dorsally and laterally overlaps the anterodorsal margin of the quadratojugal in a short scarf joint in NHMUK VP R10000, differing from the arrangement described in NMS G.1859.33.104 in which the quadratojugal externally overlaps the jugal (Clack, 1998b). There is an anteroposteriorly short butt contact between the ventral edge of the lacrimal and dorsal margin of the ectopterygoid on both sides of NHMUK VP R10000, while the lacrimal does not reach the ectopterygoid in either NHMUK PV OR30532 or in the type specimen (Clack, 1997). Similarly, the jugal does not contact the palatine in NHMUK VP R10000; however, there is an anteroposteriorly short but firm contact between the medial shelf of the jugal and the dorsolateral aspect of the posterior palatine in NHMUK PV OR30532 and the type.

Perhaps the most significant difference between specimens is the variation in the number and boundaries of the fossae (which accommodated the palatal fangs) on the dorsal surface of the lower jaw. A total of four fossae are preserved in NHMUK VP R310 and on both sides of NHMUK VP R10000, and five fossae can be visualized in GSE 4722. These fossae were first described by Panchen (1985) and subsequently figured by Ahlberg and Clack (1998) and Clack et al. (2018). Panchen (1985) stated that six fossae were present in GSE 4722; however, the most posterior fossa illustrated by Panchen (1985) appears to be due to damage. In NHMUK VP R10000 and NHMUK VP R310 the second fossa lies entirely within the dentary; in contrast, in GSE 4722, the second fossa is bounded laterally by the dentary and medially by the adsymphysial. In NHMUK VP R10000 the third fossa is bounded laterally by the dentary and medially by the anterior coronoid; however, this fossa occurs entirely within the dentary in GSE 4722. The fourth fossa is laterally bounded by the dentary and medially bounded by the middle and posterior coronoids in NHMUK VP R10000; again, this fossa lies entirely within the dentary in GSE 4722. Due to mediolateral compression, the boundaries of the first and second intercoronoid fossae are unclear in NHMUK VP R310. Whether these fossae occur entirely within the dentary, or between the dentary and coronoid series, determines whether they are homologous or analogous to the fossae observed in primitive stem tetrapods (Jeffrey, 2003; Porro et al., 2015a). An alternate explanation is that these fossae result from the opposing palatal fangs wearing through the lower jaw bone through time. Such features occur in the jaws of extant crocodilians, in which depressions caused by contact of the lower teeth with the palate are known as occlusal pits; when the teeth wear completely through the bone, the openings are termed perforations (C. Brochu personal communication, April 28, 2020). These pits and perforations are variable in occurrence, position, and depth, and it is possible that the fossae on the lower jaw of *C. scoticus*, which vary in location and depth between specimens, result from mechanical wear rather than being prepatterned by development.

The significance of the enormous, unusual interpremaxillary fenestra remains enigmatic. Its sculpted margins preclude the possibility it is simply a midline gap, as reported in other early tetrapods (Ahlberg et al., 2008; Clack, 2003; Lebedev & Clack, 1993; Pardo et al., 2017; Porro et al., 2015b). Neither Panchen (1985) nor Panchen and Smithson (1990) commented on this feature. Clack (1998b) noted that the vomer-premaxilla contact formed a solid barrier between this opening and the nasal cavity, and there is no communication between the interpremaxillary fenestra and either the external naris or the choana. It communicates with the anterior palatal fossae, and Clack (1998b) interpreted that together they formed possible exit points for the anterior dentary tusks. Although this is plausible, the vertical distance between the fossae and fenestra exceeds the height of the dentary tusks when the jaws are closed in the reconstructed skull. Furthermore, the interpremaxillary fenestra is much longer anteroposteriorly than the palatal fossae, and extends far posterior to the level of the dentary tusks. An alternative scenario presented here is that the interpremaxillary fenestra may have housed a salt gland, nasal epithelium, rostral organ or a sensory organ, such as a vomeronasal (Jacobson's) organ (Rosen et al., 1981). The latter suggestion may be supported by the paired anterior palatal fossae opening into the oral cavity, as in extant reptiles; however, it should be noted that in lungfishes and amphibians the vomeronasal organ tends to occur posterolateral to the nasal capsule in close proximity to the choanae (Rosen et al., 1981). Due to dorsoventral crushing in the two cranial specimens of *C. scoticus*, there is no clear demarcation of different regions within the anterior snout as preserved in other tetrapods (Rosen et al., 1981), thus making it difficult to pinpoint precisely which soft tissues were associated with the interpremaxillary fenestra.

Sutural Morphology

Scanning allowed visualization of sutural morphology in the upper and lower jaws (Figs. 10, 11). Sutures come in several forms, including flat-ended butt joints, overlapping scarf joints, and interdigitated joints. Experiments and computer modeling have linked certain suture shapes with specific load regimes:

butt joints are usually associated with tension and bending; interdigitated sutures are associated with compression; and scarf joints are associated with torsion, shear, or tension and compression (Busbey, 1995; Herring & Mucci, 1991; Herring & Teng, 2000; Markey et al., 2006; Rafferty & Herring, 1999). Sutural morphology has been used to predict load regimes and the feeding strategies generating these loads in various early tetrapods (Gruntmejer et al., 2019; Markey & Marshall, 2007; Porro et al., 2015a, 2015b; Rawson et al., 2021).

As noted by Clack (1998b) the bones of the anterior snout of *C. scoticus* are joined by strong interdigitating sutures. Interdigitations also occur among the bones anterior to the orbit (frontals, prefrontals), in the skull roof, and between the marginal palatal bones (vomers, palatines, and ectopterygoids) and the sidewalls of the skull (premaxilla, maxilla, lacrimal, and jugal). Butt joints are found along the entire midline of the skull roof. In contrast, the bones ventral and posterior to the orbit, and within the suspensorium, tend to meet at overlapping contacts, as does the pterygoid with the marginal palatal bones. The anterior and posterior ends of the lower jaw, as well as its dorsal margin, are dominated by strongly interdigitated contacts, especially between the adsymphysial/coronoid series and surrounding bones. The lateral and ventral aspects of the lower jaw feature overlapping scarf contacts.

Sutural morphology allows us to predict the load regime within the skull of *C. scoticus*. The strongly interdigitated joints of the marginal palate, anterior snout, and skull roof may have acted to resist and channel compressive forces from the massive palatal teeth through the robust sidewalls of the skull anterior to the orbits and to the well-consolidated skull roof. In contrast, the scarf joints of the suspensorium (posterior to the palatal dentition) may have acted to resist the complex forces generated by the jaw adductor muscles, which attached in this region, as well as reaction forces generated at the jaw joints. Midline butt joints in the skull roof suggest mediolaterally oriented tension and bending in this area, perhaps produced during unilateral biting. The interdigitated contacts at the anterior end of the lower jaw, coupled with the presence of enlarged dentary tusks and recurved adsymphysial teeth, suggests *C. scoticus* used its anterior teeth to strongly seize prey. Interdigitations between the dentary, coronoids, and prearticular may have acted to resist laterally directed forces generated by prey attempting to escape. Overlapping contacts between dentary and infradentary series would have resisted torsion and shear, which may have been crucial given potential jaw movements in *C. scoticus* (see below).

Cranial Kinesis

Previous authors have suggested various forms of kinesis within the skull of *C. scoticus*. Panchen (1973, 1975, 1985) suggested a "lateral kinetism" between the skull roof (intertemporal, supratemporal) and cheek (postorbital, squamosal) in *C. scoticus* and other early tetrapods. More recently, comparison of high-resolution CT scans of the early tetrapod *Tiktaalik* and extant taxa suggest lateral expansion of the cheek, palate, and suspensorium in this key fossil taxa during feeding (Lemberg et al., 2021). Although lacking interdigitations, the morphology (undulating butt joints) of the contacts between the skull roof and cheek in *C. scoticus* does not suggest great mobility, as Panchen (1985) himself acknowledged. Furthermore, it is unclear where movements at this joint would be accommodated elsewhere in the skull, i.e., the permissive kinematic linkages of Holliday and Witmer (2008) are lacking. The grooved and interdigitated contact between the dorsal margins of the squamosal and pterygoid effectively locked these bones together, making movement between them highly unlikely. The anterior ends of the pterygoids were extensively sutured to the vomers, and the postorbital and squamosal shared extensive overlapping contacts with the jugal, eliminating rotation or sliding at these joints. Similarly, overlapping contacts between the quadrate and the pterygoid (medially) and quadratojugal (laterally) made adjustive movements at the quadrate unlikely. Finally, strong interdigitating sutures between the marginal palatal bones and premaxilla/maxilla rule out any possibility of movements between these elements (Clack, 1996).

Beaumont (1977) proposed a unique kinetic system in loxommatids during contraction of the powerful jaw musculature, which involved deformation of the thin pterygoids, sliding movements between the pterygoids and marginal palatal bones, accommodation at the basal articulation, and rotation between the quadrate and quadratojugal. This mechanism has not been rigorously tested, and it seems unlikely to have occurred in *C. scoticus* due to the absence of a mobile joint between the quadrate and quadratojugal, as well as a strong vomer-pterygoid contact. Like many living and fossil tetrapods, *C. scoticus* features a basal articulation that was presumably synovial in life. Panchen (1985) suggested that this joint was indicative of intracranial kinesis within *C. scoticus*, and the basal articulation is a crucial element in Beaumont's (1977) palatal kinesis mechanism. However, Holliday and Witmer (2008) demonstrated that such morphology occurs widely within living tetrapods with akinetic skulls. Instead, as suggested for *Acanthostega* (Porro et al., 2015b), the basal articulation of *C. scoticus* may mark a site of growth or protected the braincase from forces generated in the facial bones or palate during feeding.

Despite isolated features suggestive of movement, the lack of convincing permissive kinematic linkages makes it unlikely that cranial kinesis occurred in *C. scoticus*.

Mandibular Symphysis, Jaw Joint, and Movements

The symphysis of *C. scoticus* consists of a circular contact surface between the dentaries, which may extend onto the adsymphysial and splenial. This symphysial surface was either flat or slightly concave, lacking any overlapping or interdigitated contacts as described in *Eusthenopteron* and *Acanthostega* (Porro et al., 2015a, 2015b). The Meckelian canal of *C. scoticus* did not open onto the symphysis, and Panchen (1985) suggested that a rugose area of the dentaries anterior to the symphysis was the site of a ligament. This suggests that the mandibular symphysis of *C. scoticus* was loose and considerable movement could occur at this contact.

Panchen (1985) previously described the complex jaw joint of *C. scoticus*: both the condyle (quadrate) and socket (articular) are saddle-shaped and posteriorly convex, and the joint surface is screw-shaped, with the medial part of the joint surface being posterodorsally directed and the lateral portion dorsally directed. Finally, as demonstrated by the new 3D reconstruction, the jaw joint was not oriented transversely but tilted anteromedially in dorsal (and ventral) view. As a result of this morphology, as suggested by Panchen (1972, 1985) and confirmed using simple physical models, during jaw opening the lower jaws rotated about their long axes, causing the tooth-bearing dorsal margins to turn outwards (laterally) while the ventral margins of the lower jaw turned inwards (medially). During jaw closure, the opposite movement occurred: the tooth row rotated inwards (medially) about the long axis of the lower jaw and the ventral margins of the lower jaw rotated outwards (laterally). Panchen (1972, 1985) suggested that these movements prevented collisions between the upper and lower teeth during jaw closure. Additionally, if the symphysis was indeed bound by an elastic ligament, jaw opening would result in stretching of and energy accumulating within the ligament; during closure, this accumulated energy would be released, assisting in jaw closure and rotation (Panchen, 1972, 1985). The overlapping scarf sutures of the lateral and ventral aspects of the lower jaw were well-adapted

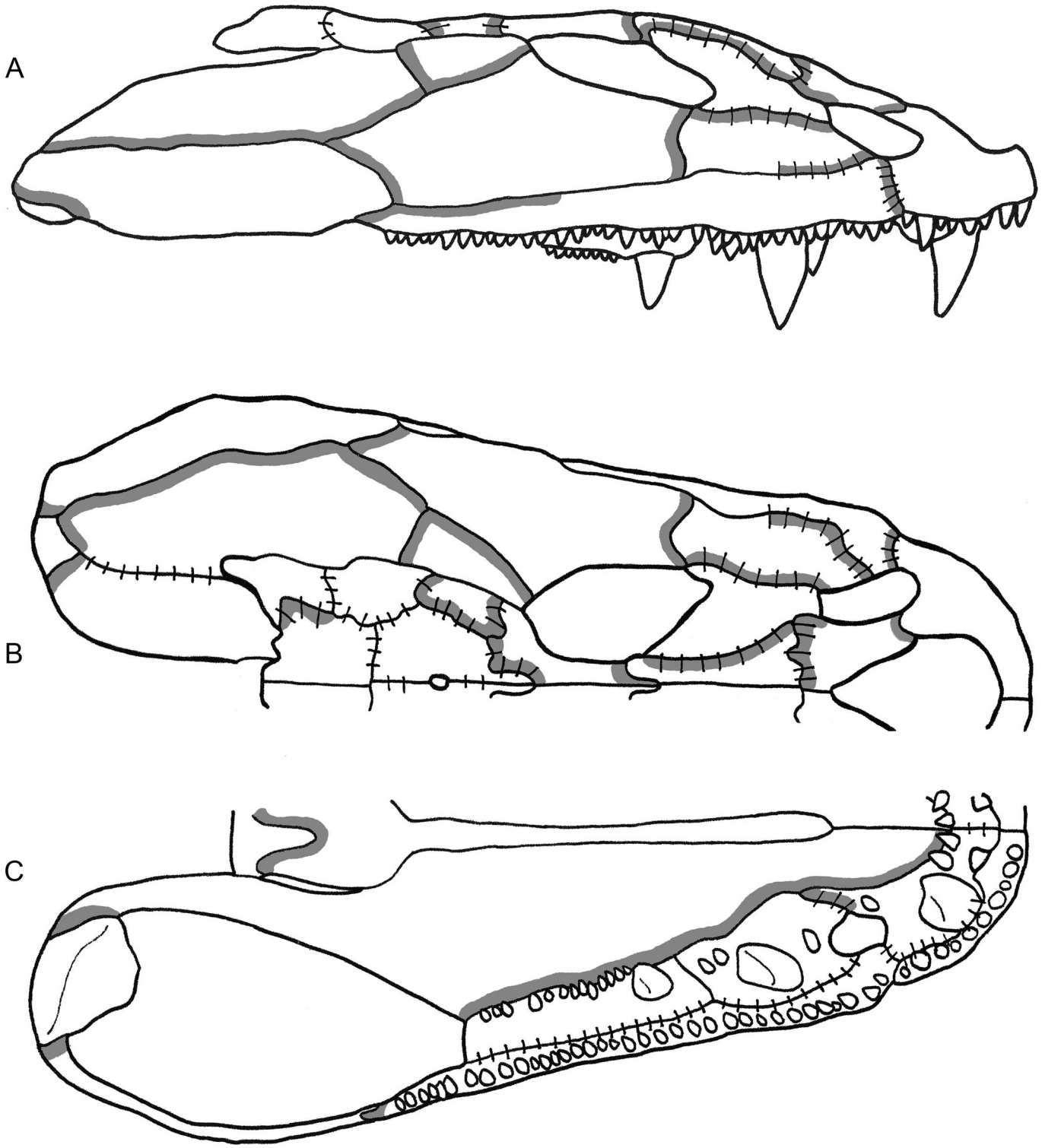

FIGURE 10. Suture maps of the cranium of *Crassigyrinus scoticus*, showing the distribution and shape of sutures. **A**, right lateral view; **B**, dorsal view (left half of cranium); **C**, ventral view (left half of cranium). Solid lines between bones indicate butt joints, shading indicates scarf joints and the direction of underlap, and hatches indicate interdigitated sutures. Not to scale.

to resist the torsion generated by long axis rotation. Furthermore, it is possible that the orientation of the jaw adductor muscles might aid in generating rotational movements; however, rigorous testing of such a hypothesis awaits reconstruction of the cranial musculature and biomechanical modeling.

Implications for Function, Diet, and Ecology

Numerous anatomical features uncovered in this study and by previous authors give insight into skull function and potential ecological niche of the enigmatic early tetrapod *C. scoticus*.

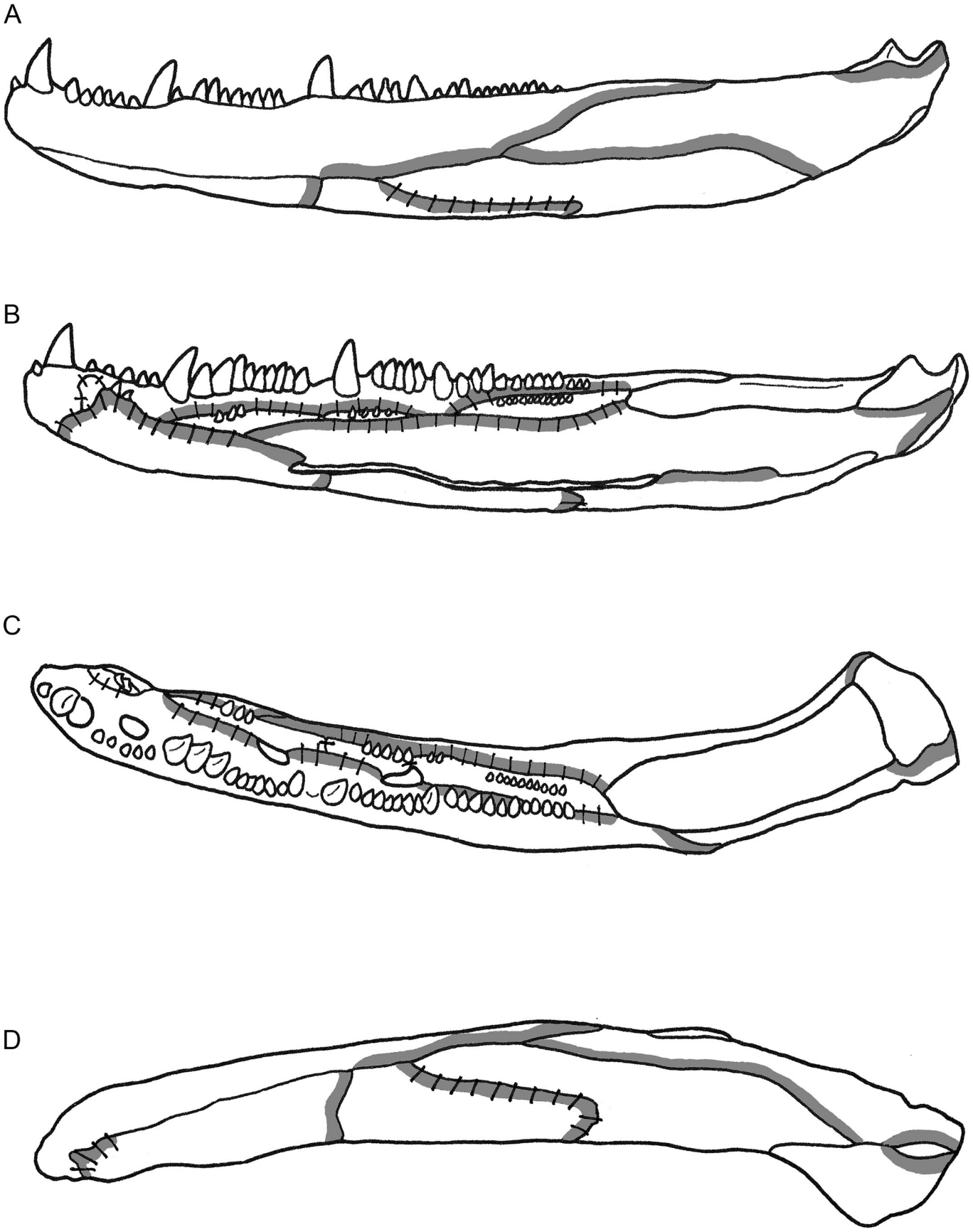

FIGURE 11. Suture maps of the lower jaw of *Crassigyrinus scoticus*, showing the distribution and shape of sutures. **A**, lateral view (of left side); **B**, medial view (of right side); **C**, dorsal view of left side; **D**, ventral view of left side. Solid lines between bones indicate butt joints, shading indicates scarf joints and the direction of underlap, and hatches indicate interdigitated sutures. Not to scale.

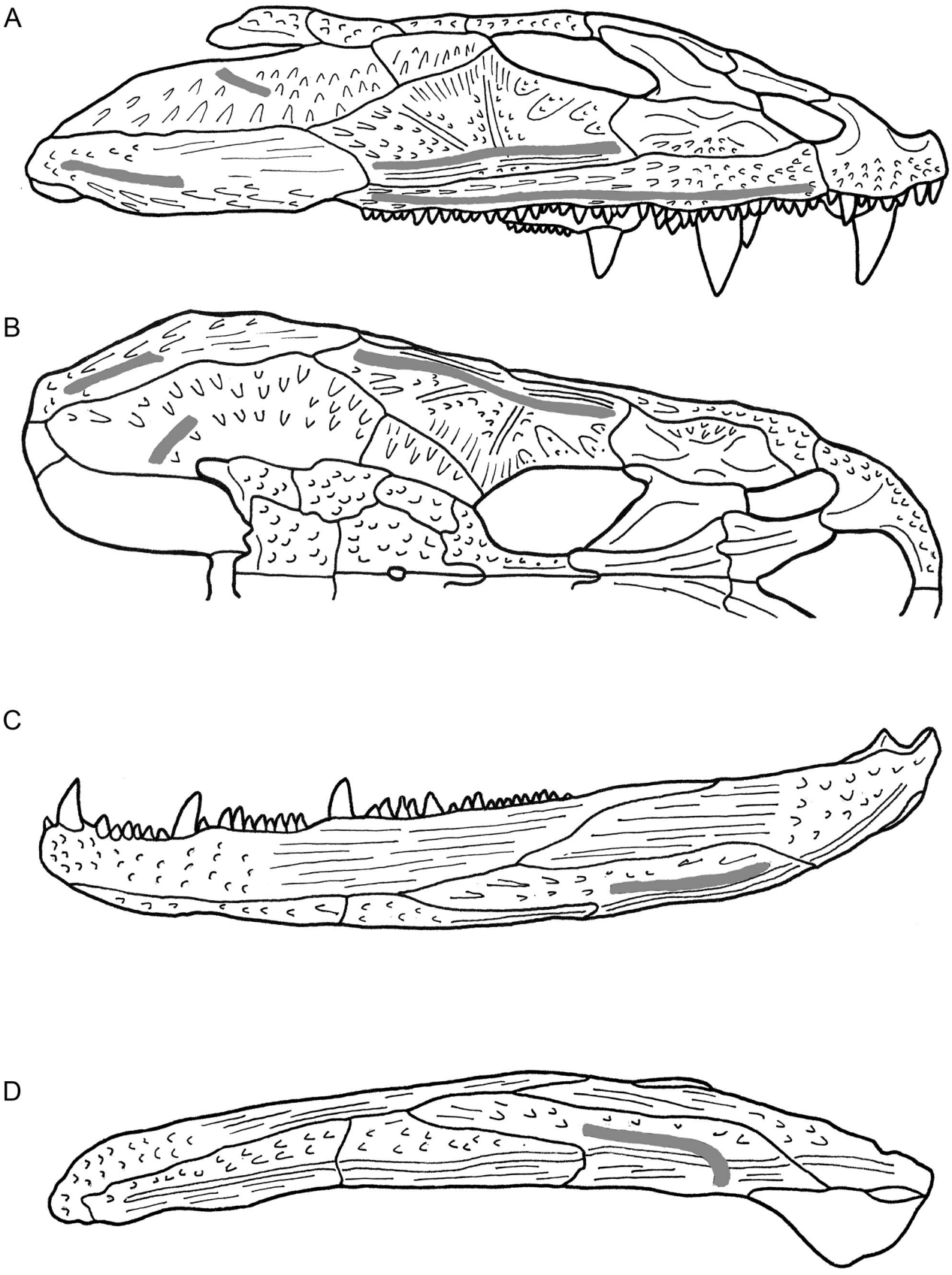

FIGURE 12. Line drawings of the upper and lower jaws of *Crassigyrinus scoticus*, showing the dermal ornamentation and course of preserved lateral line canals. **A**, right lateral view of the cranium; **B**, dorsal view (left half of cranium); **C**, lateral view of left lower jaw; **D**, ventral view of left lower jaw. Solid gray lines indicate the location of preserved lateral line canals. Not to scale.

The new 3D reconstruction is dorsoventrally shorter than previous reconstruction attempts; whereas earlier descriptions compared the skull of *C. scoticus* to that of a Moray eel, the new reconstruction is more similar in profile to the skulls of crocodilians or *Amphiuma*. This more flattened skull agrees with a recent description of the postcranial skeleton, which found that the ribs project more laterally than ventrally, and that *C. scoticus* was a fairly flat-bodied animal (Herbst & Hutchinson, 2019). The external surface of the skull features a number of strengthening ridges, including a continuous ridge along the premaxilla, nasal, and frontal, as well as ridges along the orbital margins of the prefrontal and postfrontal, which Clack (1998b) first proposed were for transmitting forces generated at the front of the skull. This idea is supported by the distribution and morphology of the cranial sutures, with strongly interdigitated sutures found in the palate, snout, and skull roof, suggesting that compressive forces generated at the anterior teeth were transferred through bones anterior to the orbit to the well-consolidated skull roof. The palatal dentition is massive, with the marginal palatal bones strongly sutured to the premaxilla and maxilla. Additionally, the tooth-bearing palatal bones are dorsally braced by the lacrimal and jugal, with CT scans revealing an internal buttress of the lacrimal immediately dorsal to the palatine fang. The reconstructed skull features enormous subtemporal fossae; the adductor muscles passed through these openings to attach to the lower jaw, suggesting *C. scoticus* possessed substantial jaw-closing musculature. All of this evidence suggests that *C. scoticus* was capable of delivering powerful anterior bites.

This proposed feeding behavior is supported by various features found in the lower jaw, including the tubular cross section of the mandible, enlarged anterior teeth, and heterodont dentition, all of which have been associated with the loss of suction feeding and ability to tackle large prey (Ahlberg & Clack, 1998). Ahlberg and Clack (1998) further suggested that the appearance of anterior dentary tusks and reorientation of the mandibular adductor fossa among early tetrapods suggest the evolution of a strong, snapping bite. The extensive overlapping contacts between the bones of the infradentary series and the appearance of the mesial lamina of the angular would have strengthened the floor of the mandibular adductor fossa for the insertion of powerful jaw muscles, as well as compensating for the loss of the Meckelian bone (Ahlberg & Clack, 1998). The undulations of the dorsal margin of the lower jaw and associated heterodonty of the dentary teeth are features found in extant crocodilians, some dinosaurs, and some fish, and have been linked to capturing aquatic prey. The jaw mechanism first proposed by Panchen (1972, 1985), involving long axis rotation of the lower jaws during opening and closing, appears to have been possible in *C. scoticus* due to anatomical modifications of the jaw joint and mandibular symphysis. Furthermore, it should be noted that the dentary teeth are medially curved; thus, inward rotation of the tooth row during closure coupled with tooth shape would have aided penetration of a prey item. Lastly, *C. scoticus* possessed an unusually elongated suspensorium, first noted by Watson (1929), resulting in a posteriorly displaced jaw joint. This would have permitted a wide maximum gape angle—Clack (1998b) predicted a maximum gape of over 60°—as well as fast jaw closure. Although further biomechanical testing is required, the evidence presented here suggests that *C. scoticus* employed fast snapping movements—a kinetic inertial system of feeding as proposed by Olson (1961)—to capture aquatic prey, and was potentially able to tackle large prey through strong biting (powered by expanded jaw adductor muscles) at enlarged palatal and anterior dentary teeth, the bone-shattering bites proposed by Clack (1998b, 2012).

A final brief note will be made of the sensory systems of *C. scoticus* and their implications for ecology. As observed by previous authors, *C. scoticus* possessed relatively large orbits, which in the new reconstruction are shown to have faced dorsolaterally. As detailed in the Description, the upper and lower jaws were covered with sulci and pores of the lateral line system; these were especially densely distributed near the tooth rows and at the anterior ends of the jaws (Fig. 12). Lastly, it is cautiously suggested here that the unusual interpremaxillary fenestra of *C. scoticus*, which communicated with the anterior palatal fossae, may have (among other potential functions) housed a salt gland, nasal epithelium, and/or a rostral, vomeronasal, or other sensory organ. All of these sensory systems would have aided *C. scoticus* in hunting prey in its coal swamp habitat. Together with evidence from the postcranial skeleton (Panchen & Smithson, 1990; Herbst & Hutchinson, 2019), our results paint a picture of *C. scoticus* as a large aquatic predator using its powerful, fast bite to capture large prey.

CONCLUSIONS

The results presented here supplement and amend previous descriptions of *C. scoticus*, including new information on skull anatomy, sutural morphology, and a detailed description of the jaw joint and mandibular symphysis. Computed tomography and 3D visualization permitted a new 3D reconstruction of the upper and lower jaws of *C. scoticus.* The reconstructed cranium is dorsoventrally flatter than previous attempts and features a vaulted palate and enormous subtemporal fossae; the new lower jaw is less curved than earlier reconstructions, and the jaw joint is anteromedially tilted rather than transversely oriented. Evidence from skull anatomy, sensory systems, tooth size, shape and distribution, sutural morphology, and the shape and orientation of the jaw joint and mandibular symphysis are used to predict the feeding mechanism and ecology in this unusual stem tetrapod, hypotheses that will be tested further using biomechanical modeling.

ACKNOWLEDGMENTS

This paper is dedicated to the memory of our coauthor, colleague and friend J. A. Clack, who passed away on March 26, 2020. Jenny worked extensively on *Crassigyrinus* during her career and we are grateful for her knowledge and support in this project and many others. Thanks to S. Chapman (Natural History Museum), M. Lowe (University of Cambridge), and S. Wild (British Geological Survey) for access to specimens, S. Wallace-Johnson (formerly Finney) (University of Cambridge) for specimen preparation, and D. Sykes (Natural History Museum) and T. Davies, B. Moon, and L. Martin-Silverstone (University of Bristol) for μCT scanning at the University of Bristol XTM Facility. Many thanks to J. Hutchinson (Royal Veterinary College) and E. Herbst (Universität Zürich) for sharing CT data of NHMUK VP R10000 containing the displaced basioccipital and right skull roof. Thanks to C. Janis (Brown University/University of Bristol) and T. Smithson (University of Cambridge) for insights into the functional significance of various anatomical features of *Crassigyrinus*, M. Ruta (University of Lincoln) for discussions of early tetrapod phylogeny, and C. Brochu (University of Iowa), C. Holliday (University of Missouri), and H.-D. Sues (Smithsonian National Museum of Natural History) for discussion on the occurrence of occlusal pits and perforations in crocodilians. A. Sánchez-Eróstegui and J.-L. Garnier (Thermo Fisher Scientific) provided technical support for Avizo. We would like to thank the handling editor A. Huttenlocker and three anonymous reviewers for their insight and constructive suggestions, which helped improve the manuscript. This work was funded by NERC (Natural Environment Research Council) Standard Grant NE/P013090/1 to E.J.R. and L.B.P. and Marie Curie International

Incoming Research Fellowship ("Tetrapods Rising", 303161) to L.B.P.

ORCID

Laura B. Porro http://orcid.org/0000-0002-0546-2381
Emily J. Rayfield http://orcid.org/0000-0002-2618-750X
Jennifer A. Clack http://orcid.org/0000-0003-0017-5831

LITERATURE CITED

Ahlberg, P. E. (1995). *Elginerpeton pancheni* and the earliest tetrapod clade. *Nature*, *373*, 420–425.

Ahlberg, P. E., & Clack, J. A. (1998). Lower jaws, lower tetrapods—a review based on the Devonian genus *Acanthostega*. *Transactions of the Royal Society of Edinburgh: Earth Sciences*, *89*, 11–46.

Ahlberg, P. E., Clack, J. A., & Blom, H. (2005). The axial skeleton of the Devonian tetrapod *Ichthyostega*. *Nature*, *437*, 137–140.

Ahlberg, P.E., Clack, J. A., Luksevics, E., Blom, H., & Zupin, I. (2008). *Ventastega curonica* and the origin of tetrapod morphology. *Nature*, *453*, 1199–1204.

Ahlberg, P. E., Luksevics, E., & Lebedev, O. A. (1994). The first tetrapod finds from the Devonian (Upper Famennian) of Latvia. *Philosophical Transactions of the Royal Society of London B*, *343*, 303–328.

Anderson, P. S. L., Friedman, M., Brazeau, M. D., & Rayfield, E.J. (2011). Initial radiation of jaws demonstrated stability despite faunal and environmental change. *Nature*, *476*, 206–209.

Anderson, P. S. L., Friedman, M., & Ruta, M. (2013). Late to the table: diversification of tetrapod mandibular biomechanics lagged behind the evolution of terrestriality. *Integrative and Comparative Biology*, *53*, 197–208.

Arbez, T., Atkins, J. B., & Maddin, H. C. (2022). Cranial anatomy and systematics of *Dendrerpeton* cf. *helogenes* (Tetrapoda, Temnospondyli) from the Pennsylvanian of Joggins, revisited through micro-CT scanning. *Papers in Palaeontology*, *8*, Article e1421. https://doi.org/10.1002/spp2.1421

Ashley-Ross, M. A. (1994). Hindlimb kinematics during terrestrial locomotion in a salamander (*Dicampton tenebrosus*). *Journal of Experimental Anatomy*, *193*, 255–283.

Beaumont, E. I. (1977). Cranial morphology of the Loxommatidae (Amphibia: Labyrinthodontia). *Philosophical Transactions of the Royal Society of London B*, *280*, 29–101.

Beznosov, P. A., Clack, J. A., Lukševičs, E., Ruta, M., & Ahlberg, P. E. (2019). Morphology of the earliest reconstructable tetrapod *Parmastega aelidae*. *Nature*, *574*, 527–531.

Boisvert, C. A., Makr-Kurik, E., & Ahlberg, P. E. (2008). The pectoral fin of *Panderichthys* and the origin of digits. *Nature*, *456*, 636–638.

Bolt, J. R., & Lombard, R. E. (2001). The mandible of the primitive tetrapod *Greererpeton* and the early evolution of the tetrapod lower jaw. *Journal of Paleontology*, *75*, 1016–1042.

Bolt, J. R., & Lombard, R. E. (2010). *Deltaherpeton hiemstrae*, a new colosteid tetrapod from the Mississippian of Iowa. *Journal of Paleontology*, *84*, 1135–1151.

Bolt, J. R., & Lombard, R. E. (2018). Palate and braincase of *Whatcheeria deltae* Lombard and Bolt. *Earth and Environmental Science Transactions of the Royal Society of Edinburgh*, *109*, 177–200.

Busbey, A. P. (1995). The structural consequences of skull flattening in crocodilians. In J.J. Thomason (Ed.), *Functional Morphology in Vertebrate Paleontology* (pp. 173–192). Cambridge University Press.

Callier, V., Clack, J. A., & Ahlberg, P. E. (2009). Contrasting developmental trajectories in the earliest known tetrapod forelimbs. *Science*, *324*, 364–367.

Clack, J. A. (1989). Discovery of the earliest-known tetrapod stapes. *Nature*, *342*, 425–427.

Clack, J. A. (1992). The stapes of *Acanthostega* and the role of the stapes in early tetrapods. In D. B. Webster, R. R. Fay, & A. N. Popper (Eds.), *The Evolutionary Biology of Hearing* (pp. 405–420). Springer-Verlag.

Clack, J. A. (1994). Earliest known tetrapod braincase and the evolution of the stapes and fenestra ovalis. *Nature*, *369*, 392–394.

Clack, J. A. (1996). The palate of *Crassigyrinus scoticus*, a primitive tetrapod from the Lower Carboniferous of Scotland. *Special Papers in Palaeontology*, *52*, 55–64.

Clack, J. A. (1998a). The neurocranium of *Acanthostega gunnari* Jarvik and the evolution of the otic region in tetrapods. *Zoological Journal of the Linnean Society*, *122*, 61–97.

Clack, J. A. (1998b). The Scottish Carboniferous tetrapod *Crassigyrinus scoticus* (Lydekker) – cranial anatomy and relationships. *Transactions of the Royal Society of Edinburgh: Earth Sciences*, *88*, 127–142.

Clack, J. A. (2002a). An early tetrapod from 'Romer's Gap'. *Nature*, *418*, 72–76.

Clack, J. A. (2002b). Patterns and processes in the early evolution of the tetrapod ear. *Journal of Neurobiology*, *53*, 251–264.

Clack, J. A. (2003). A revised reconstruction of the dermal skull roof of *Acanthostega gunnari*, an early tetrapod from the Late Devonian. *Transactions of the Royal Society of Edinburgh: Earth Sciences*, *93*, 163–165.

Clack, J. A. (2009). The fin to limb transition: new data, interpretations, and hypotheses from paleontology and developmental biology. *Annual Review of Earth and Planetary Sciences*, *37*, 163–179.

Clack, J. A. (2012). *Gaining ground: the origin and evolution of tetrapods*. Indiana University Press.

Clack, J. A., Ahlberg, P. E., Blom, H., & Finney, S. M. (2012). A new genus of Devonian tetrapod from North-East Greenland, with new information on the lower jaw of *Ichthyostega*. *Palaeontology*, *55*, 73–86.

Clack, J. A., Bennett, C. E., Carpenter, D. K., Davies, S. J., Fraser, N. C., Kearsey, T. I., Marshall, J. E. A., Milward, D., Otoo, B. K. A., Reeves. E. J., Ross, A. J., Ruta, M., Smithson, K. Z., Smithson, T. R., & Walsh, S. A. (2016). Phylogenetic and environmental context of a Tournasian tetrapod fauna. *Nature Ecology and Evolution*, *1*, 1–11.

Clack, J. A., Porro, L. B., & Bennett, C. E. (2018). A *Crassigyrinus*-like jaw from the Tournasian (Early Mississippian) of Scotland. *Earth and Environmental Sciences Transactions of the Royal Society of Edinburgh*, *108*, 37–46.

Clack, J. A., Ruta, M., Milner, A. R., Marshall, J. E. A., Smithson, T. R., & Smithson, K. Z. (2019). *Acherontiscus caledoniae:* the earliest heterodont and durophagus tetrapod. *Royal Society Open Science 6*, Article 182087. https://doi.org/10.1098/rsos.182087

Coates, M. I. (1996). The Devonian tetrapod *Acanthostega gunnari* Jarvik: poscranial anatomy, basal tetrapod interrelationships and patterns of skeletal evolution. *Transactions of the Royal Society of Edinburgh: Earth Sciences*, *87*, 363–421.

Coates, M. I., & Clack, J. A. (1990). Polydactyly in the earliest known tetrapod limbs. *Nature*, *347*, 66–69.

Coates, M. I., Ruta, M., & Friedman, M. (2008). Ever since Owen: Changing perspectives on the early evolution of Tetrapods. *Annual Review of Ecology, Evolution and Systematics*, *39*, 571–592.

Cunningham, J. A., Rahman, I. A., Lautenschlager, S., Rayfield, E. J., & Donoghue, P. C. (2014). A virtual world of paleontology. *Trends in Ecology and Evolution*, *29*, 347–357.

Daeschler, E. B., Shubin, N. H., & Jenkins, F. A. (2006). A Devonian tetrapod-like fish and the evolution of the tetrapod body plan. *Nature*, *440*, 757–763.

Deakin, W. J., Anderson, P. L., Boer, W. D., Smith, T. J., Hill, J. J., Rücklin, M., Donoghue, P. C. J., & Rayfield, E. J. (2022). Increasing morphological disparity and decreasing optimality for jaw speed and strength during the radiation of jawed vertebrates. *Science Advances*, *8*, Article eabl3644. https://doi.org/10.1126/sciadv.abl3544

Dickson, B. V., Clack, J. A., Smithson, T. R., & Pierce, S. E. (2021). Functional adaptive landscapes predict terrestrial capacity at the origin of limbs. *Nature*, *589*, 242–245.

Dutel, H., Herbin, M., Clement, G., & Herrel, A. (2015). Bite force in the extant coelacanth *Latimeria*: the role of the intracranial joint and the basicranial muscle. *Current Biology*, *25*, 1228–1233.

Dutel, H., Herrel, A., Clement, G., & Herbin, M. (2013). A reevaluation of the anatomy of the jaw-closing system in the extant coelacanth *Latimeria chalumnae*. *Naturwissenschaften*, *100*, 1007–1022.

Esteve-Altava, B., Pierce, S. E., Molnar. J. L., Johnston. P., Diogo, R., & Hutchinson, J. R. (2019). Evolutionary parallelism of pectoral and pelvic network-anatomy from fins to limbs. *Science Advances*, *5*, Article eaau7459. https://doi.org/10.1126/sciadv.aau7459

Fortuny, J., Marce-Nogue, J., Heiss, E., Sanchez, M., Gil, L., & Galobart, A. (2015). 3D bite modeling and feeding mechanics of the largest living amphibian, the Chinese giant salamander *Andrias davidianus* (Amphibia: Urodela). *PLoS One*, *10*, Article e121885. https://doi.org/10.1371/journal.pone/0121885

Fortuny, J., Marce-Nogue, J., & Konietzko-Meier, D. (2017). Feeding biomechanics of Late Triassic metoposaurids (Amphibia : Temnospondyli): a 3D finite element analysis approach. *Journal of Anatomy*, *230*, 752–765.

Godfrey, S. J. (1988). Isolated tetrapod remains from the Carboniferous of West Virginia. *Kirtlandia*, *43*, 27–36.

Gradstein, F. M., Ogg, J. G., Schmitz, M., & Ogg, G. (2012). *The Geologic Time Scale 2012*. Elsevier.

Gregory, W. K., & Raven, H. C. (1941). Studies on the origin and early evolution of paired fins and limbs. *Annals of the New York Academy of Sciences*, *42*, 275–361.

Gruntmejer, K., Konietzko-Meier, D., Marcé-Nogué, J., Bodzioch, A., & Fortuny, J. (2019). Cranial suture biomechanics in *Metoposaurus krasiejowensis* (Temnospondyli, Stereospndyli) from the upper Triassic of Poland. *Journal of Morphology*, *280*, 1850–1864.

Heiss, E., Natchev, N., Gumpenberger, M., Weissenbacher, A., & Van Wassenbergh, S. (2013). Biomechanics and hydrodynamics of prey capture in the Chinese giant salamander reveal a high-performance jaw-powered suction feeding mechanism. *Journal of the Royal Society Interface*, Article 10:20121028. https://doi.org/10.1098/rsif.2012.1028

Herbst, E. C., & Hutchinson, J. R. (2019). New insights into the morphology of the early Carboniferous tetrapod *Crassigyrinus scoticus* from computed tomography. *Earth and Environmental Science Transactions of the Royal Society of Edinburgh*, *109*, 157–175.

Herring, S. W., & Mucci, R. J. (1991). *In vivo* strain in cranial sutures: the zygomatic arch. *Journal of Morphology*, *207*, 225–239.

Herring, S. W., & Teng, S. (2000). Strain in the braincase and its sutures during function. *American Journal of Physical Anthropology*, *112*, 575–593.

Holliday, C. M., & Witmer, L. M. (2008). Cranial kinesis in dinosaurs: intracranial joints, protractor muscles, and their significance for cranial evolution and function in dinosaurs. *Journal of Vertebrate Paleontology*, *28*, 1073–1088.

Hook, R. W. (1983). *Colosteus scultellatus* (Newberry), a primitive temnospondyl amphibian from the Middle Pennsylvanian of Linton, Ohio. *American Museum Novitates,* 2770, 1–41.

Jarvik, E. (1980). *Basic Structure and evolution of vertebrates*. Academic Press.

Jeffrey, J. E. (2003). Mandibles of rhizodontids: anatomy, function and evolution within the tetrapod stem-group. *Transactions of the Royal Society of Edinburgh: Earth Sciences*, *93*, 255–276.

King, H. M., Shubin, N. H., Coates, M. I., & Hale, M. E. (2011). Behavioural evidence for the evolution of walking and bounding before terrestriality in sarcopterygian fishes. *Proceedings of the National Academy of Sciences of the United States of America*, *108*, 21146–21151.

Lautenschlager, S. (2016). Reconstructing the past: methods and techniques for the digital restoration of fossils. *Royal Society Open Science*, *3*, Article 160342. https://doi.org/10.1098/rsos.160342

Lautenschlager, S., Witzmann, F., & Werneburg, I. (2016). Palate anatomy and morphofunctional aspects of interpterygoid vacuities in temnospondyl cranial evolution. *Naturwissenschaften*, *103*, 79.

Lebedev, O. A., & Clack, J. C. (1993). Upper Devonian tetrapods from Andreyevka, Tula Region, Russia. *Palaeontology*, *36*, 721–734.

Lemberg, J. B., Daeschler, E. B., & Shubin, N. H. (2021). The feeding system of *Tiktaalik rosae:* an intermediate between suction feeding and biting. *Proceedings of the National Academy of Sciences, 118*, Article e2016421118. https://doi.org/10.1073/pnas.201642118

Lennie, K., Mansky, C., & Anderson, J. (2020). New *Crassigyrinus*-like fibula from the Tournasian (earliest Carboniferous) of Nova Scotia. *Canadian Journal of Earth Sciences*, *57*, 1365–1369.

Lydekker, R. (1890). On two new species of labyrinthodonts. *Quarterly Journal of the Geological Society of London*, *46*, 289–294.

MacIver, M. A., Schmitz, L., Mugan, U., Murphey, T. D., & Mobley, C. D. (2017). Massive increase in visual range preceded the origin of terrestrial vertebrates. *Proceedings of the National Academy of Sciences of the United States of America*, *114*, 2375–2384.

Markey, M. J., Main, R. P., & Marshall, C. D. (2006). *In vivo* cranial suture function and suture morphology in the extant fish *Polypterus:* implications for inferring skull function in living and fossil fish. *Journal of Experimental Biology*, *209*, 2085–2012.

Markey, M. J., & Marshall, C. R. (2007). Terrestrial-style feeding in a very early aquatic tetrapod is supported by evidence from experimental analysis of suture morphology. *Proceedings of the National Academy of Sciences of the United States of America*, *104*, 7134–7138.

Milner, A. R., & Sequeira, S. E. K. (1994). The temnospondyl amphibians from the Vísean of East Kirkton, West Lothian, Scotland. *Transactions of the Royal Society of Edinburgh: Earth Sciences*, *84*, 331–361.

Mogdans, J. (2019). Sensory ecology of the fish lateral-line system: morphological and physiological adaptations for the perception of hydrodynamic stimuli. *Journal of Fish Biology*, *95*, 53–72.

Molnar, J. L., Hutchinson, J. R., Diogo, R., Clack, J. A., & Pierce, S. E. (2021). Evolution of forelimb musculoskeletal function across the fish-tetrapod transition. *Science Advances*, *7*, Article eabd7457. DOI:10.1126/sciadv.abd7457.

Neenan, J. M., M. Ruta, J. A. Clack, and E. J. Rayfield. 2014. Feeding biomechanics in *Acanthostega* and across the fish-tetrapod transition. Proceedings of the Royal Society B 281:20132689. https://doi.org/10.1098/rspb.2013.2689

Olson, E. C. (1961). Jaw mechanisms: rhipidistians, amphibians, reptiles. *American Zoologist*, *1*, 205–215.

Panchen, A. L. (1972). The skull and skeleton of *Eogyrinus attheyi* Watson (Amphibia: Labyrinthodontia). *Philosophical Transactions of the Royal Society of London*, *263*, 279–326.

Panchen, A. L. (1973). On *Crassigyrinus scoticus* Watson, a primitive amphibian from the Lower Carboniferous of Scotland. *Palaeontology*, *16*, 179–193.

Panchen, A. L. (1975). A new genus and species of anthracosaur amphibian from the Lower Carboniferous of Scotland and the status of *Pholidogaster pisciformis* Huxley. *Philosophical Transactions of the Royal Society of London*, *269*, 581–640.

Panchen, A. L. (1985). On the amphibian *Crassigyrinus scoticus* Watson from the Carboniferous of Scotland. *Philosophical Transactions of the Royal Society of London*, *309*, 505–568.

Panchen, A. L., & Smithson, T. R. (1990). The pelvic girdle and hind limb of *Crassigyrinus scoticus* (Lydekker) from the Scottish Carboniferous and the origin of the tetrapod pelvic skeleton. *Transactions of the Royal Society of Edinburgh: Earth Sciences*, *81*, 31–44.

Pardo, J. D., Szostakiwskyj, M., Ahlberg, P. E., & Anderson, J. S. (2017). Hidden morphological diversity among early tetrapods. *Nature*, *546*, 642–645.

Pierce, S. E., Ahlberg, P. E., Hutchinson, J. R., Molnar, J. L., Sanchez, S., Tafforeau, P., & Clack, J. A. (2013). Vertebral architecture in the earliest tetrapods. *Nature*, *494*, 226–229.

Pierce, S. E., Clack, J. A., & Hutchinson, J. R. (2012). Three-dimensional limb joint mobility in the early tetrapod *Ichthyostega. Nature*, *486*, 523–526.

Porro, L. B., Rayfield, E. J., & Clack, J. A. (2015a). Computed tomography, anatomical description and three-dimensional reconstruction of the lower jaw of *Eusthenopteron foordi* Whiteaves, 1881 from the Upper Devonian of Canada. *Palaeontology*, *58*, 1031–1047.

Porro, L. B., Rayfield, E. J., & Clack, J. A. (2015b). Descriptive anatomy and three-dimensional reconstruction of the skull of the early tetrapods *Acanthostega gunnari* Jarvik, 1952. *PLoS ONE*, *10*, Article e0124731. https://doi.org/10.1371/journal.pone.0124731

Rafferty, K. L., & Herring, S. W. (1999). Craniofacial sutures: morphology, growth, and In Vivo masticatory strain. *Journal of Morphology*, *242*, 167–179.

Rawson, J. R. G., Porro, L. B., Martin-Silverstone, E., & Rayfield, E. J. (2021). Osteology and digital reconstruction of the skull of the early tetrapod *Whatcheeria deltae. Journal of Vertebrate Paleontology*, *41*, Article e1927749. https://doi.org/10.1080/02724634.2021.1927749

Rosen, D. E., Forey, P. L., Gardiner, B. G., & Patterson, C. (1981). Lungfishes, tetrapods, paleontology, and plesiomorphy. *Bulletin of the American Museum of Natural History*, *167*, 159–276.

Ruta, M., Coates, M. I., & Quicke, D. L. J. (2003). Early tetrapod relationships revisited. *Biological Reviews*, *78*, 251–345.

Schwarz, D., Konow, N., Porro, L. B., & Heiss, E. (2020). Ontogenetic plasticity in cranial morphology associated with a change in the food processing behavior in Alpine newts. *Frontiers in Zoology*, *17*. https://doi.org/10.1186/s12983-020-00373-x

Simões. T. R., & Pierce, S. E. (2021). Sustained high rates of morphological evolution during the rise of tetrapods. *Nature Ecology and Evolution*, *5*, 1403–1414.

Smithson, T. R. (1982). The cranial morphology of *Greererpeton burkemorani* Romer (Amphibia: Temnospondyli). *Zoological Journal of the Linnean Society*, *76*, 29–90.

Standen, E. M., Du, T. Y., & Larsson, H. C. E. (2014). Developmental plasticity and the origin of tetrapods. *Nature*, *513*, 54–58.

Watson, D. M. S. (1929). The Carboniferous Amphibia of Scotland. *Palaeontologia Hungarica*, *1*, 219–252.

Handling Editor: Adam Huttenlocker.